CFD ANALYSIS OF FLOW PATTERN IN ELECTROCHEMICAL MACHINING FOR L-SHAPED TOOL

A thesis
Submitted by

Baburaj M
(210ME2242)

In partial fulfillment of the requirements
for the award of the degree of

Master of Technology
In
Mechanical Engineering
(Production Engineering)

Department of Mechanical Engineering
National Institute of Technology Rourkela
Orissa -769008, India
May 2012

CFD ANALYSIS OF FLOW PATTERN IN ELECTROCHEMICAL MACHINING FOR L-SHAPED TOOL

A thesis
Submitted by

Baburaj M
(210ME2242)

In partial fulfillment of the requirements
for the award of the degree of

Master of Technology
In
Mechanical Engineering
(Production Engineering)

Under The Guidance of
Dr. C.K. Biswas

Department of Mechanical Engineering
National Institute of Technology Rourkela
Orissa -769008, India
May 2012

NATIONAL INSTITUTE OF TECHNOLOGY
ROURKELA – 769008, ORISSA
INDIA

This is to certify that the thesis entitled, "**CFD Analysis of Flow Pattern in Electrochemical Machining for L-Shaped Tool**" submitted by **Baburaj M** in partial fulfillment of the requirement for the award of **Master of Technology** degree in **Mechanical Engineering** with specialization in **Production Engineering** at the National Institute of Technology, Rourkela is an authentic work carried out by her under my supervision and guidance. To the best of my knowledge, the matter embodied in the thesis has not been submitted to any other University/Institute for the award of any degree or diploma.

Research Guide

Place: Rourkela
Date:

Dr. C.K. Biswas
Associate Professor
Department of Mechanical Engineering
NIT Rourkela

ACKNOWLEDGEMENTS

First and foremost, praise and thanks goes to my God for the blessing that has bestowed upon me in all my endeavors.

I am deeply indebted to **Dr. C.K. Biswas,** my advisor and guide, for the motivation, guidance, tutelage and patience throughout the research work. I appreciate his broad range of expertise and attention to detail, as well as the constant encouragement he has given me over the years. There is no need to mention that a big part of this thesis is the result of joint work with him, without which the completion of the work would have been impossible.

I am grateful to **Prof. K.P. Maity**, Head, Department of Mechanical Engineering for his valuable suggestions during the synopsis meeting and for the unyielding support over the year.

My family members, they played a great roll in my carrier and their love and support has been a major stabilizing force till this moment.

My friends, **Miss. Bijily B, Mr. Shiba narayan Sahoo, Mr. Akhilesh and Mr. Shailesh Devangan,** I remembering their support and helps in this occasion with great pleasure.

So many people have contributed to my thesis, to my education, and to my life, and it is with great pleasure to take the opportunity to thank them. I apologize, if I have forgotten anyone.

Baburaj M

ABSTRACT

KEYWORDS: *CFD, ECM, flow pattern, IEG, MRR, passivation, temperature profile*

Electrochemical machining is a non-conventional machining process worked with a principle of Faraday's law. Due to improper tool design of complicated shapes, there are chances of passivation and boiling of electrolyte in ECM process that causes poor machining. Predicting the flow pattern is also important to prevent boiling tendency of electrolyte is due to overheating of electrolyte. This project work is for optimizing the design of L-shaped tool and to study the flow pattern, current density distribution, velocity profile, temperature pattern, turbulence and final shape change of workpiece top surface. Four models with different shaped grooves for supplying electrolyte are evaluated.

ANSYS-CFX software was used for simulating this CFD problem. Geometrical model consists of a circular workpiece made with Iron, 20% brine solution as electrolyte and L-shaped copper tool with different kind of grooves. This problem is considered as a steady-state problem with turbulence model. A potential difference of 10V is applied in between the IEG. The models were simulated for various inlet velocities and the major findings are stated below.

The maximum temperature in IEG for all models has a decreasing tendency with respect to the increase in inlet velocities. The maximum current density has increasing tendency with respect to increase in inlet velocities. MRR and turbulence also increase in inlet velocities. Tendency of passivation is decreasing in case of all models with increasing velocity. Model 3 is the best tool design from among the four models evaluated.

TABLE OF CONTENTS

Title **Page No.**

Title **Page No**

Title **Page No**

Title **Page No**

LIST OF TABLES

Title **Page No**

LIST OF FIGURES

Title **Page No**

Title **Page No**

Title **Page No**

ABBREVIATIONS

BEM	Boundary Element Method
CAE-ECM	Computer Aided Engineering System for ECM
CEL	CFX Expression Language
CEM	Computational Electro Magnetics
CFD	Computational Fluid Dynamics
CHT	Conjugate Heat Transfer
DEM	Discrete Element Method
ECM	Electrochemical Machining
ECM -E	Electrochemical Machining Envelope
EHD	Electro Hydro Dynamics
FDM	Finite Difference Method
FEM	Finite Element Method
GGI	General Grid Interface
IEG	Inter Electrode Gap
MeTis	Multilevel Graph Partitioning Software
MHD	Magneto Hydro Dynamics
MRR	Material Removal Rate
RANS	Reynolds Averaged Navier-Stokes
RNG	Re-Normalisation Group
SOFC	Solid Oxide Fuel Cell
SPMD	Single Program Multiple Data

NOTATIONS

a	Area of element
A	Atomic weight
A_1	Area at inlet
C_p	Specific heat capacity
Δd	Deformation of nodes
Δv	Over voltage
Δt	Time step
E	Electric field
ε	Current efficiency
F	Faradays constant
F_{emag}	Coulomb force
h	Height of node from workpiece top surface
i	Specified turbulence intensity
I	Current
J	Current density
k	Thermal conductivity of electrolyte
k_0	Initial thermal conductivity of electrolyte
l	Edge length of tetrahedron
λ	Thermal conductivity
m	Weight of material dissolved or deposited
μ_{eff}	Effective viscosity for turbulent
μ_t	Turbulent viscosity

$P^{'}$	Modified pressure
P_k	Turbulent production due to viscous force
P_{kb} & $P_{\varepsilon b}$	Influence of buoyancy forces
q	Electric charge
Q	Volume flow rate
S_m	Sum of body force
t	Total machining time
T	Temperature of control volume
T_b	Boiling temperature of electrolyte
v	Velocity at inlet
V	Potential difference applied across electrode
V_r	Volume of machined region
y	Inter electrode gap
z	Valancy

CHAPTER 1

INTRODUCTION

1.1. OVERVIEW OF ECM PROCESS

Electrochemical machining (ECM) is a method based on electrochemical process for removing metals in mass productions. It is working with hard materials which are impossible for conventional machining process. The ECM is a reverse of electroplating and similar to electrical discharge machine (EDM). However ECM is not using any tool wear and the cutting tool is not in touch with the specimen at the time of machining unlike EDM. Due to the complex behavior it also has some demerit like week degree of accuracy makes a specimen shape has slit difference from the actual shape of the specimen. This method is useful for all conducting metals. Now a day we use high strength, low weight metallic and intermetallic alloys for many applications. High cutting forces and imperfection in cutting give low preference to conventional milling and turning process. This is uneconomical too due to tool wear and low machining rates. Here the importance of ECM comes. In case of complicated shapes of workpiece it's very difficult to know the machining variables distribution within the inter electrode gap (IEG). So there is a need to understand about those parameters. Once we are aware about flow pattern then it's easy to avoid passivation. Passivation is one of the major difficulties in ECM process in the case of complicated shapes. This is the motivation behind this project.

1.2. WORKING PRINCIPLE

Electrochemical machining removes material from the work piece by electrochemical process.

The working principle is anodic dissolution in which the work piece as anode and the tool as cathode. Both electrodes are immersed in the electrolyte and electrical applied to these electrodes. The electric conduction is achieved through the movements of ions between the anode and cathode through the electrolyte. The current is passing through the system of arrangements will cause the dissolution of anode. This process of electrolysis is working based on Faradays law of electrolysis. The principal and process detailing of ECM for steel is shown in Figures 1.1 and 1.2, generally a neutral salt solution of sodium chloride (NaCl) is taken as the electrolyte.

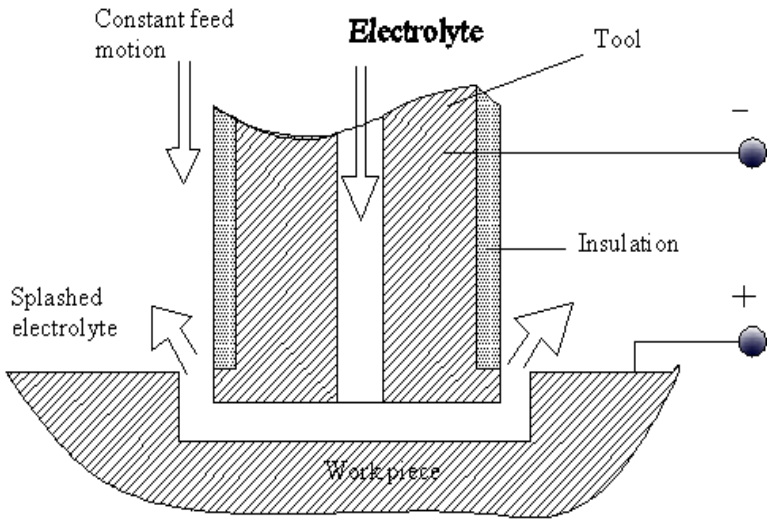

Fig. 1.1: Principle of Electrochemical Machining

Reaction occurring in the anode shown in Figure 1.2 is demonstrated as follows,

$$Fe \leftrightarrow Fe^{2+} + 2e^{-}$$

$$Fe^{2+} + 2Cl \leftrightarrow FeCl_2$$

$$Fe^{2+} + 2OH^{-} \leftrightarrow Fe(OH)_2$$

$$FeCl_2 + 2OH^- \leftrightarrow Fe(OH)_2 + 2Cl^-$$

$$2Cl^- \leftrightarrow Cl_2 \uparrow + 2e^-$$

$$2FeCl_2 + Cl_2 \leftrightarrow 2FeCl_3 \downarrow$$

$$H^+ + Cl^- \leftrightarrow HCl$$

$$2Fe(OH)_2 + H_2 + O_2 \leftrightarrow 2Fe(OH)_3 \downarrow$$

$$Fe(OH)_3 + 3HCl \leftrightarrow FeCl_3 + 3H_2O$$

$$FeCl_3 + 3NaOH \leftrightarrow Fe(OH)_3 \downarrow + 3NaCl$$

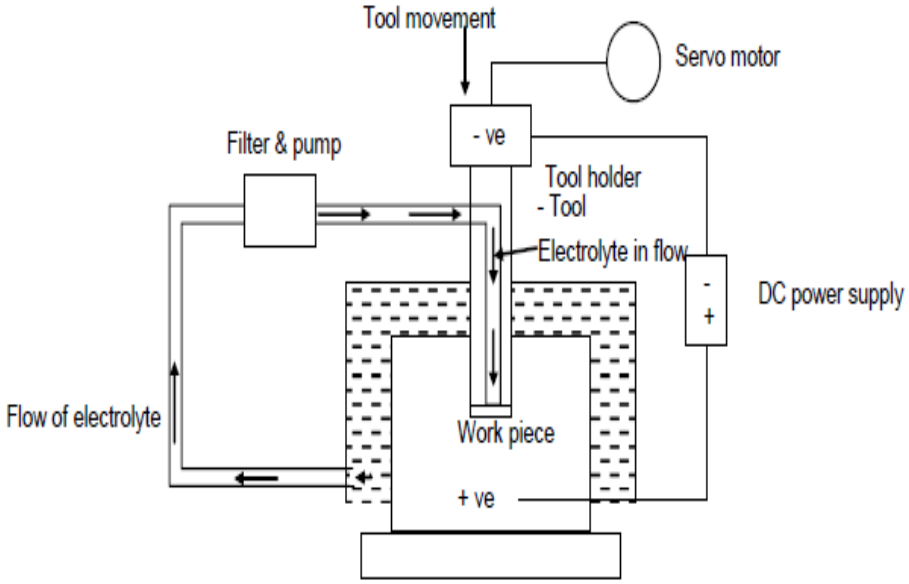

Fig. 1.2: Process details of Electrochemical Machining

In cathode the reaction is given below,

$$Na^+ + e^- \leftrightarrow Na$$

$$Na + H_2O \leftrightarrow NaOH + H^+ \uparrow$$

$$2H^+ + 2e^- \leftrightarrow H_2 \uparrow$$

1.2.1. Material Removal

Electrolysis is the basis of material removal. Faraday suggested two laws for this, first one is "the amount of chemical change produced by an electric current, which is the amount of any material dissolved or deposited, is proportional to the quantity of electricity passed". Second is "The amount of different substances dissolved by the same quantity of electricity are proportional to their chemical equivalent weights". Quantitative form of Faradays law is given in Equation 1.1

$$m = \frac{ItA}{\rho zF} \tag{1.1}$$

If anode is an alloy metal instead of pure metal then removal rate can be found out by considering the rate required to remove a unit volume of each element. If atomic weight and the valences are A_1, A_2, $A3$ etc. and Z_1, Z_2, Z_3 etc. respectively and composition by weight of the alloy x_1% of alloy 1, x_2 % of alloy 2 etc. then a volume v cm^3 of the alloy contains $v\rho x_i/100$ gram of the i^{th} element. Charge required to remove the entire i^{th} element in the volume v is given by the Equation 2.2.

$$Q = \frac{100}{\rho F}\left(\frac{1}{\Sigma_i\left(\frac{x_i Z_i}{A_i}\right)}\right) \tag{1.2}$$

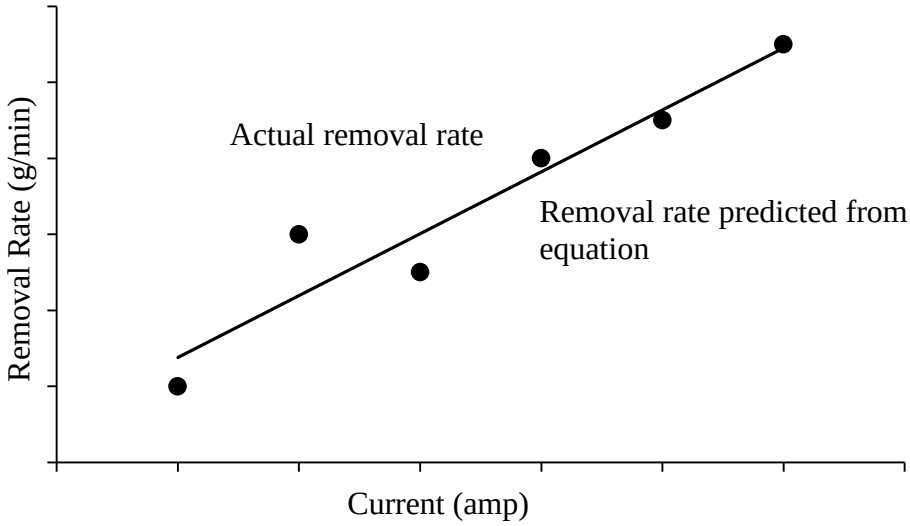

Fig. 1.3: Removal rate versus current for nickel

In actual ECM process many factors are affecting the material removal rate. But the theoretical removal rate based on divalent dissolution only. When the current is more sometimes the dissolution takes place at higher potential and trivalent dissolution is also happening. The removal rate versus the current for nickel is shown in the Figure 1.3. Therefore theoretical value tends to be more than actual one. Sometimes dissolution valance is also affecting the material removal rate (MRR). For example in the case of copper dissolved in chloride solution in monovalent form and in nitrate solutions it is in the divalent state.

1.2.2. Workpiece

Work piece is functioning as an anode and is connected with positive terminal of the direct current (DC) power supply. The anodic dissolution will remove the material from the workpiece in the presence of pressurized electrolyte between the electrodes in a set temperature.

1.2.3. Tool

Tool is connected with the negative terminal of the supply (Cathode). Basic chemistry reveals cathode dissolution rate is very less compared to anode, so tool have more life span. Generally tool is made with copper, brass, stainless steel etc. Proper allowances are given for avoiding the taper and over cut etc.

1.2.4. Power Supply

DC power supply is used with low voltage and high current.

1.2.5. Electrolyte

Electrolyte are conductive fluid has an important functional role in ECM. Continues current flow between the anode and cathode is made possible with the electrolyte by completing the electrical circuit. It keeps the electrodes cool and removes the machined particle from the electrode. Generally water soluble NaCl or $NaNO_3$ are used as electrolyte. Mainly using electrolyte corresponding to the alloy is explained in the Table 1.1.

Table.1.1: Type of electrolytes

Sl No.	Alloy	Electrolyte
1	Iron based	Chloride solutions in water (mostly 20% NaCl)
2	Ni based	HCl or mixture of brine and H_2SO_4
3	Ti based	10% hydrofluoric acid+10% HCl+10% HNO_3
4	Co-Cr-W based	NaCl
5	WC based	Strong alkaline solutions

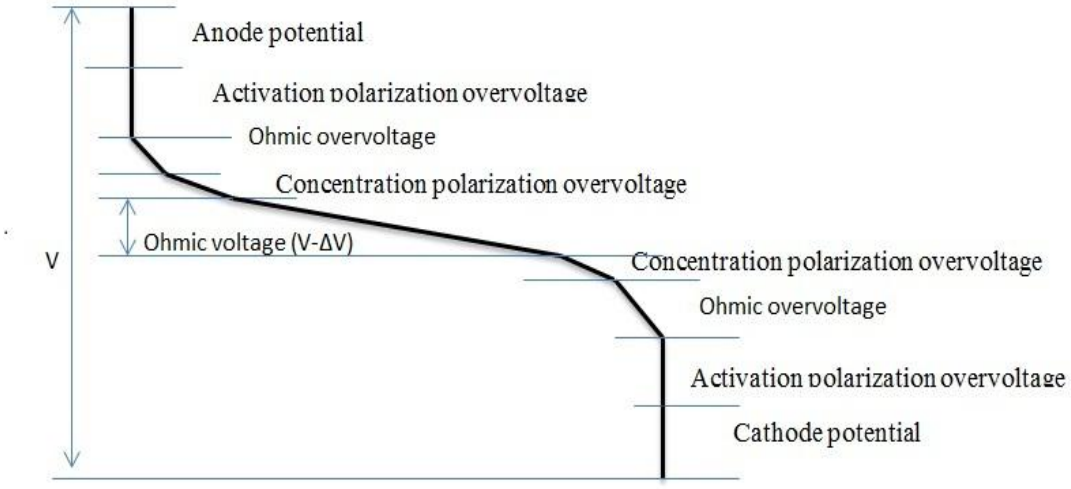

Fig. 1.4: Potential drop in ECM cell

Voltage is required to apply for electrochemical reaction around 2 to 30V. This applied voltage is required to overcome the potential drop or voltage drop between the electrodes are shown in the Figure 1.4.

i) Electrode potential

Electrode potential is nothing but cathode and anode potential.

ii) Over voltage due to activation polarization

The minimum potential difference needed to break the equilibrium condition or steady state to start current flow in the circuit is called activation polarization.

iii) Concentration polarization

Ions are accumulated near to the electrodes and it act as a barrier. The extra voltage required for breaking this barrier is called concentration polarization.

iv) Ohmic overvoltage.

Thin films formed in the electrodes during the machining will offer extra resistance. This effect is called ohimc overvoltage.

v) Ohmic resistance of electrolyte.

Electrical resistance offered by the electrolyte is called ohmic resistance of electrolyte. This is the main voltage drop obey Ohm's law.

1.2.6. Electrolyte Flow

Insufficient electrolyte flow in IEG will cause poor machining. The effect of cavitation, stagnation, and vortex flow can avoid up to a certain extent by avoiding sharp corner. The entire flow path has an approximate radius of 0.7 to 0.8 mm. Flow will not cover all area of the workpiece at starting. That can avoid by using restriction techniques. Figure 1.5 shows a tool with no sharp corners.

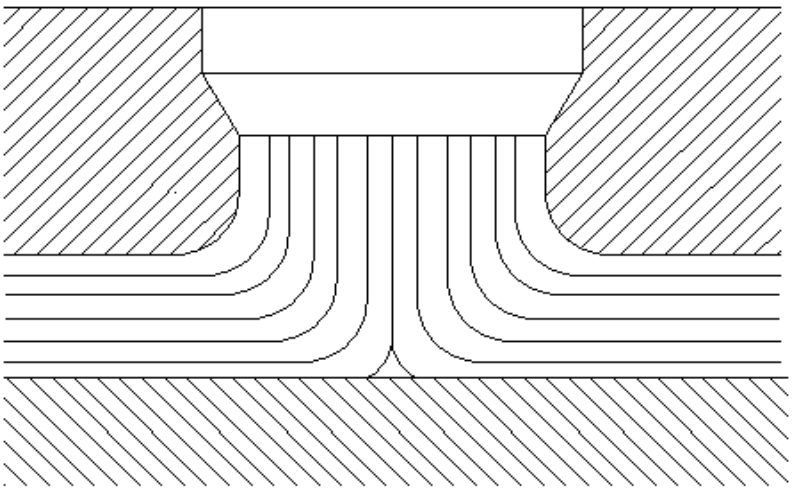

Fig. 1.5: Tool with no sharp corners

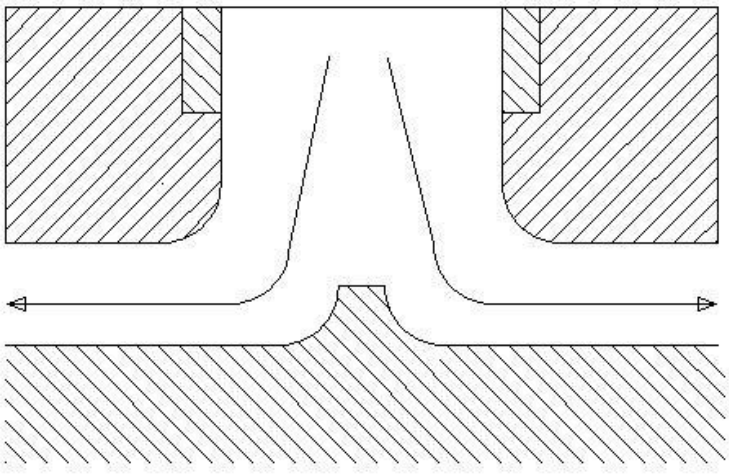

Fig. 1.6: Boss formation in machining

Sometimes the formation of boss or ridges during machining helps to distribute electrolyte in the proper manner. Figures 1.6 and 1.7 present the boss and ridge formation during machining. In the case of complicated shapes electrolyte supply through slots are helps to supply sufficient electrolyte in the IEG.

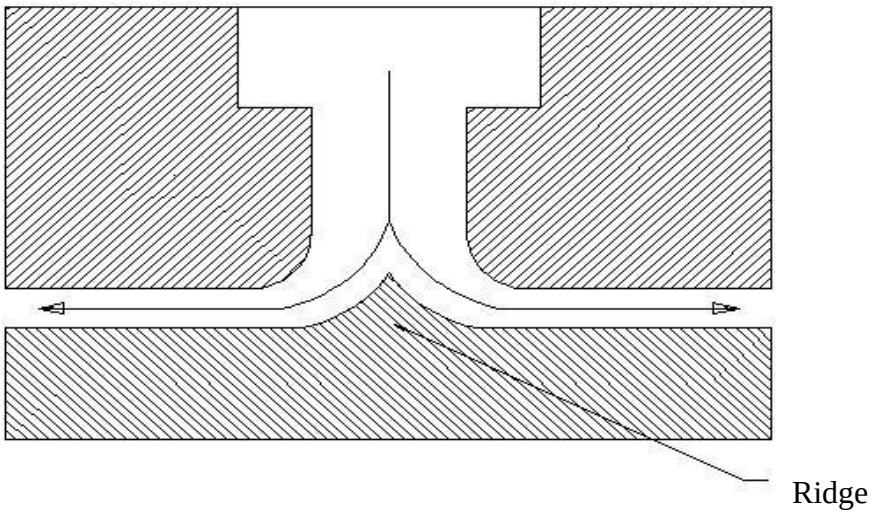

Fig. 1.7: Ridge formation in machining

Smooth ridges will form when we gave sufficiently narrow slot in the tool. Flow from thew slots are always perpendicular to the slots and at the end it always showing poor flow. So we want to stop that groove befor the workpiece edge. Normally distance from the end of the slots to the corner of the workpiece is atleast 1.5 mm and slot with a recommended width of 0.8 mm as like in the Figure 1.8. If the workpiece corner is rounded then the end of the groove also made larger as like in the Figure 1.9. These things will help to avoid creation of passivated area. If the slot positions are wrong that causes creation of passivated area. Formation of passivated area is shown in Figures 1.10 and 1.11.

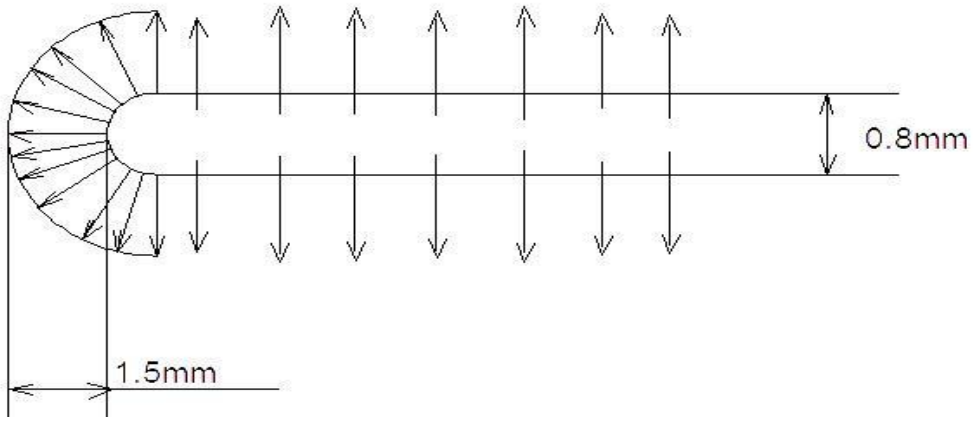

Fig. 1.8: Slot with sharp corner

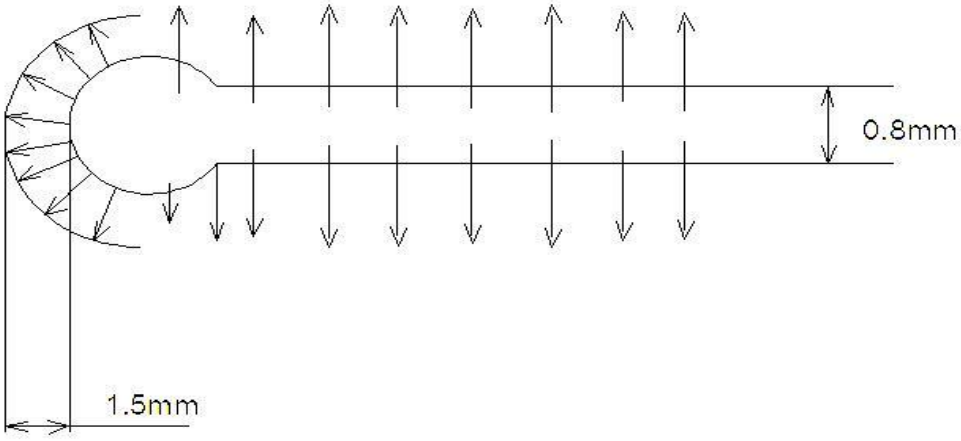

Fig. 1.9: Slot without Sharp corner.

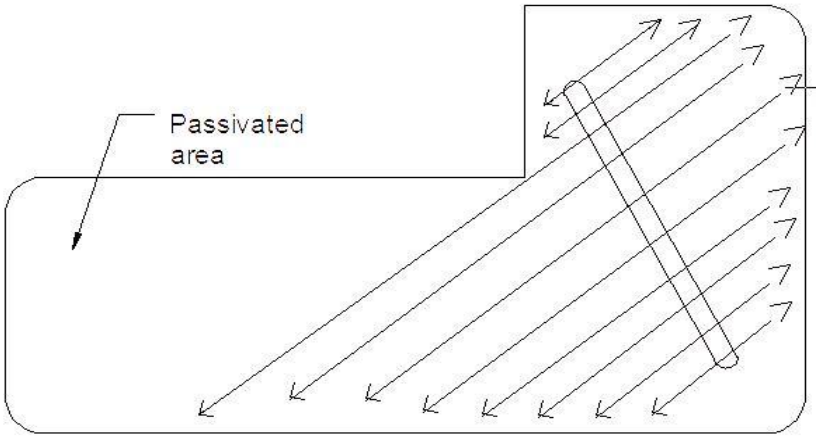

Fig. 1.10: Passivation due to flow interruption.

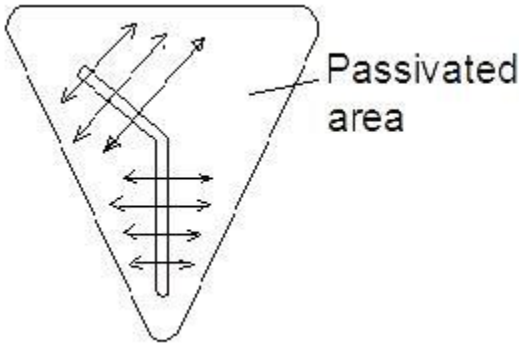

Fig. 1.11: Passivation due to sharp bend in slot.

Passivated area is occurring due to insufficient flow of electrolyte. Figure 1.10 and 1.11 is corrected as the Figure 1.12 and 1.13 to avoid. In some cases for making accurate surfaces reverse flow tool type are used, but for more complicated shapes it is expensive.

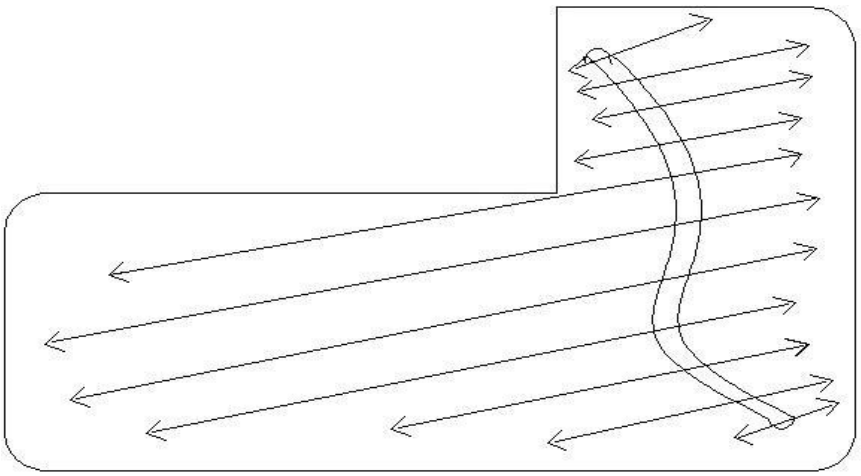

Fig. 1.12: Correct slot arrangement for model Fig. 1.10

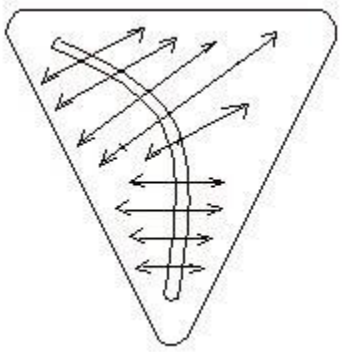

Fig. 13: Correct slot arrangement for model Fig. 1.11

1.3. ORGANIZATION OF THESIS

This introductory chapter presents the basis of ECM. The basic principal and models of tools are presented in this chapter.

Chapter 2 reviews the previous work done on ECM since 1974. This research works are given the motivation for the presented study. The objectives and scope of the proposed research work are identified in this chapter.

Chapter 3 presents computational modelling of selected buildings using ANSYS. The model details also explained in this chapter.

Chapter 4 presents the results obtained from analyses of the selected models along with the discussions on these results.

Finally, in Chapter 5, the summary and conclusions are presented. The scope for future work is also discussed.

CHAPTER 2

LITERATURE REVIEW

2.1. INTRODUCTION

A detailed literature review is carried out on Electrochemical Method (ECM). It is found that research on this topic started way back in 1969. These previous works are discussed in this chapter. The total literatures are grouped as BEM and, FEM and FDM methods. Some other literature related to other tooling methods also explained in this chapter. The scope and objective of the current study is presented in this chapter.

2.2. LITERATURE REVIEW

The works on ECM is using different analytical and numerical methods. Thorpe and Zerkle (1969) discussed about the effect of void fraction and temperature variation of the electrolyte. But the limitation of this is restricted to one dimensional workpiece shape only. McGeough (1974) introduce Sine rule analytical technique for analysing shape change of electrode. Main drawback of this technique is neglecting stray current effects and they assume that flux lines are parallel. Kozak *et al.* (1998) discussed about the computer simulation electrochemical shaping using a universal tool electrode; its application is limited in Flexible Manufacturing System. In this paper universal electrode tool for avoiding the difficulties in ECM and the final shape of the workpiece is obtained by controlling the motion of tool. This study is to avoid the usage of high cost electrodes with complicated shapes. Another advantage of this is to reduce the working area,

so the heat generated and gas formation was reduced and also the dissolution rate was also more uniform. ECM-E is a best tool to solve the tool controlling problem. Alder *et al.* (2000) used another analytical model, direct computation of 2DECM based on Fourier's series. Battacharya *et al.* (2002) uses Boolean logic based control system for controlling the inter electrode gap. This is a nonlinear and complex process so it is very difficult to develop a mathematical model.

Marius Purcar *et al*. (2004) discussed about 3D electrochemical machining computer simulation based on marker method. This method related with the instantaneous change of tool shape. Kang Min, Tang Xinyan and X U Jiawen (2006) published a paper on analysis of the shaping law of numerical controlled electrochemical counter evolution machining [NE-ECEM]. In this paper, the shaping law of machining grooves by using inner spraying cathode with triangular cross-section is explained. the cathode movement is expressed with a differential equation and found the bottom gap and side gap while machining vertical, inclined and circular grooves. In the case of bottom gaps the experimental results and the calculated results are in good agreement. In the case of side gap calculated is larger than the actual value but the change trend in both are coincide with each other.

N Krimmelbein and R Radespiel (2009) published a paper related to the transition prediction for three dimensional flows, in that they used parallel computation technique. The necessary requirement of a three dimensional complex computational flow is to predict and model the laminar-turbulent transition in Reynolds-averaged Navier-Stokes solvers, because transition from laminar to turbulent is a complicated phenomenon. In this technique hybrid approach is used to calculate the transition prediction. The main aim of this paper is to give an idea about development and parallelization of the transition module and the application in 3D complex

flows. The DLR Tau code is used as Navier-Stokes solver for calculation of viscous and in viscid flows around the general flows.

A W Labib *et al.* (2011) present a literature about the new generation ECM controllers. This paper discussed about the use of Fuzzy system for controlling the ECM process. The main thing is in the ECM process is the inter electrode gap, with the help of Fuzzy logic we can give the property of artificial intelligence and easily control the inter electrode gap. Use of Fuzzy logic controller may result more consistent level of performance. The input parameters are voltage, current, measured flow rate, electrolyte conductivity and electrolyte temperature. Mat lab software is used for creating Fuzzy program. The aim of fuzzy logic control is to keep the ECM process with in the optimum area of control. If there is any variation shown in the fuzzy logic, it will help to come back to the optimum condition. Another important parameter in the ECM process is the condition of electrolyte. If the condition of electrolyte is bad also Fuzzy technique will encourage the results and give good results because its interaction is simultaneous.

Guermond and Minev (2011) published a paper related to the direction splitting algorithm for the incompressible Navier-Stokes equation. This paper is using an operator for approximating the pressure correction instead of Poisson operator. The marching algorithms used to solve large scale incompressible fluid flow problems. The main objective of his paper is to introduce a novel fractional time stepping technique. This technique is very much help to simplify pressure equation now they to simplify the momentum equation using the same, because it will reduce the overall complexity of the problem. The new program consists of a singular perturbation of the Navier-Stokes equations by using an operator ‘A’. They set different value of ‘A’ in two space

and three-space dimensions. The time dependent Stokes equation is written in the form of pressure ($Ap^{n+\frac{1}{2}}=-\frac{1}{\Delta t}\nabla.u^{n+1}$) and velocity is explained in Equation 2.1.

$$\begin{cases} \partial_t u - v\nabla u + \nabla p = f in\Omega\nabla \times [0,\mathrm{T}], \\ \nabla . u = 0 \quad in\Omega \times [0,\mathrm{T}], \\ u \mid \partial\Omega = 0 \ \text{ in } [0,\mathrm{T}], \quad \text{and u } \mid_{\mathrm{t=0}\ \text{ in } \Omega,} \end{cases} \tag{2.1}$$

This technique is proposed only for simple domains. In future may be this will use for complex problems.

2.2.1. Finite Element And Finite Difference Method

The papers used finite element methods (FEM) and finite difference methods (FDM) for modeling tool or workpiece is explained in this section. These methods are using since 1982 for modeling ECM problems. Prentice and Tobias (1982) used finite different method (FDM) with primary, secondary and tertiary current density distribution .They prove that the electrode shape change is a function of Wagner's number.

Brookes (1984), Jain *et al.* (1987) and Hardisty *et al.* (1993) used FEM for predicting tool shape. Hourng and Chang (1993) introduce more realistic FDM model. They used FDM for two phase flow of electrolyte and FEM methods for solve potential problem.

Kozak (1998) proposed a Mathematical model for computer simulation of electrochemical machining process. Software for the ECM process was developed in Warsaw University of Technology covered the basic manufacturing problems in ECM. This software includes FDM, FEM, and BEM techniques for solving the problem. In this paper the Physical and Mathematical model based on simulation module are presented. This software is called CAE-ECM. The assumptions used for this are three IEG regions are defined (region with pure electrolyte, bubble

region, region of two-phase flow). Second one is current density depends up on the shape of electrode and electrolyte conductivity and the last one is surface tension effect on the gas bubble is neglected etc.

Mount *et al*. (2003) used two techniques for the data collection for ECM experiment. First one is that the use of planar workpiece and planar tool configuration for theory analysis and second one is planar segment tool-planar workpiece ECM system. The current in the process is obtained from the Equation 2.2 below

$$\frac{I_\infty}{A} = \frac{nf\rho F}{M} \text{ and } \frac{dz}{dt} = k\left[\frac{1}{z} - \frac{1}{z_\infty}\right] \tag{2.2}$$

On integrating Equation (2.2), where, I_∞ = Current when t= ∞. And f=$\frac{dy}{dt}$

$$ln\left[\frac{1-(I_\infty/I_i)}{1-(I_\infty/I)}\right] + \left[\frac{I_\infty}{I_i} - \frac{I_\infty}{I}\right] = \frac{k(t-t_i)}{z_\infty^2} = \frac{f^{2(t-t_i)}}{k} \tag{2.3}$$

For this experiment workpiece used is In718 alloy with an initial gap of 0.8mm.In this experiment produce a close agreement between theoretical and experimental data. From this experiment they found out that f^2/k and I_i are the important parameters and these will help to find out the value of V_0. Finite different simulation is used here and assumes that changes in the electric field distribution within the gap occurring in the workpiece. Here also they used Laplace field equation. It shows some deviations in between the theory and experiment. To get a better simulation they introduce planar segmented tool-planar workpiece ECM system. They expect that the composition of electrolyte change at slower flow rate and higher ECM current because of the changes in conception and production of ions. Planar segmented tool system means the planar tool is split up into number of parts (here it is seven). The current passing through each

segment (In) is measured separately. In this experiment first and last segment shows deviation from theoretical solution because of the overlapping with the workpiece. This technique is also used in the case of change in valance along the electrolyte path length. The change in valance due to the variation in composition in the electrolyte during the process is explained.

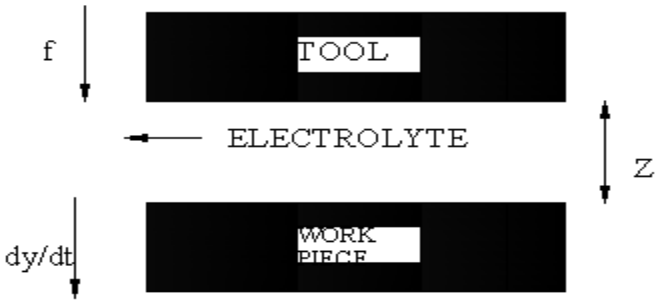

Fig. 2.1: The configuration for ECM

T. Gambaryan-Roisman and P. Stephan (2006) studied about the thermo capillarity-induced flow of thin liquid films covering heated horizontal walls with 2D topography. This presents the 2D solution of heat and fluid flow in liquid film, gas above the film and the structured wall. Finite difference method is used for solving all Navier-Stokes equation. They found out that the convective motion with in a structured wall is existing when all non-zero Marangoni number. This solution is only used in the case of periodic wall structures and flow. This is very much good for design heat transfer equipment. In the liquid gas interface they used Volume of Flow concepts. They present some numerical model for solving this kind of problem.

2.2.2. Boundary Element Method

The introduction of boundary element method (BEM) solves the difficulties in FEM and FDM for ECM modeling. The works related to this method is explained in this section. Narayanan *et al.* (1986) used this technique to predict 2D shape of workpiece in drilling. Kozak (2000) used this method for spherical tools. In this Boundary element model, they used rectangular tool, hollow open topped box like work piece and an inverted U shaped channel. Current density distribution on the tool and work piece is represented by Laplace's Equation 2.4.

$$\nabla^2 u = 0 \tag{2.4}$$

For this experiment three slots are made, one is narrow, next is deeper and the last one is wider. Here single pass with varying time steps are considered for analysing the effect of time step in accuracy. In 10s time steps it shows 11% error and $\Delta t \leq 4.5$s boundary element results converges. The deeper slot shows a good agreement with the experimental and analytical data, here the error is less than 2%. It shows good agreement in the Centre and rounded profiles in the corners because of the reduced amount of electrolyte in this region. In the case of wider slots the base surface is flat and wall surfaces are smooth. A small degree of waviness is there, that depends up on the step over distance. If the step over distance reduced to 0.1mm the waviness reduced and the smoothness increases. In that 80% is used for calculating the element matrices and 20% for solving the equations.

Leslie Bortels *et al.* (2004) discussed about a simulation software tool for 3D ECM. That simulation software fully integrated within the CAD package (Solid Works). The main advantage of this software is the geometrical entities are readily available. With the help of this software, they construct a complete reactor. In this paper, they used 3D BEM for the potential

distribution and 2D FEM techniques for Ohmic potential drops. For BEM model, for unknown potential and flux field they used Laplace equation and triangular element with linear shape functions. The same meshing is used for 2D FEM also. Matrix representation for resistive electrode is explained in Equation 2.5.

$$\varpi[Y].\{V\} + [R].\{J_n\} = \{I_{ext}\} \tag{2.5}$$

They coupled these equations with a boundary condition there is no current on insulators

$$\begin{bmatrix} [H] & {}^{1}/_{\sigma[-G]} & [0] \\ [0] & [I] & [0] \\ [0] & [R] & \varpi[Y] \end{bmatrix} \begin{Bmatrix} \{U\} \\ \{j_n\} \\ \{V\} \end{Bmatrix} + \begin{Bmatrix} \{0\} \\ \{f(V-U)\} or \{0\} \\ -(I_{ext}) \end{Bmatrix} = 0 \tag{2.6}$$

Newton-Rapson method was used for solving nonlinear equations and for linear equations an iterative algorithm is used. Accuracy depends up on meshing so a hybrid grid generator is used for both BEM and FEM. It creates structured or unstructured mesh for each surface separately. Here they conduct two experiments one is die making and other is cavity formation, both simulation gives better results. Usage of this software enables the direct integration of creating hybrid grids and applied boundary conditions. Obtained conclusion is that powerful 3D simulation Software can reduce designing time of ECM.

Most recently Purcar *et al*. (2004) developed BEM software to model 3D ECM process. Trial and error method are using for predicting the workpiece shape. Some analytical models are used for this. Pattavanitch *et al.* (2010) discussed about modeling of the electrochemical machining process by the boundary element method (BEM).

2.2.3. Computational Fluid Dynamics

The past works related to Computational Fluid Dynamic (CFD) are presented here. M. Pons and P. Le Que´re (2006) worked on the topic modeling natural convection with the work of pressure-forces. They used thermodynamically consistent Boussinesq model (i.e. still assuming v=0) for maintaining the heat equation. Undimensional quantities are used for thermodynamic model. Buoyance induced convection is not considered in this study and entropy model getting from UB model is also not correct are considered as the disadvantages of this system.

L Dabrowski and T Paczkowski (2011) published paper related to the two dimensional electrolyte flows in ECM. They used vibrating type tool for machining. They found out that the usage of vibrating tool helped to increase accuracy and stability of machining. During machining the IEG alter from minimum to maximum according to the current density. The physical phenomena in IEG are described by using differential equation and partial derivatives. Shape of the workpiece is altered due to non-uniform rate of anodic dissolution. Temperature distribution in the IEG with a constant feed depends up on the hydrodynamic conditions. They concluded that at lower vibration frequencies calculated results are more accurate.

Guilan Wang *et al.* (2007) publish an article about 3-D model of thermo-fluid and electrochemical for planar SOFC. They solved Thermo fluid model using ANSYS-CFX. A repeating unit of SOFC units constructed having a positive electrode, negative electrode, electrolyte and an interconnecting stack is provided. In this simulation, solid and fluid domains are divided in to discrete meshes. For each meshes, conservation equation of species, mass, momentum and energy equations were applied. The species conservation equation is given Equation 2.7.

$$\nabla(\rho C_k U) = \nabla\left(D_{k,eff}\nabla C_k\right) + I_k, K = H_2, O_2, H_2O \quad (2.7)$$

The boundary conditions they used are, cell units are repeating and having a middle stack, and external walls are assumed as adiabatic and in the case of inlet fuel and air the boundary constant temperature, delivery rate etc. Here they used electrochemical equations used for solving this problem.

Ratkovich *et al*. (2009) discussed about two-phase flow in their experiment. There is a possibility of two-phase flow in ECM process because there is an emission of Hydrogen gas while doing machining. After so many studies it is found that changing the flow direction and corresponding change in the direction of the induced surface shear stress will minimize fouling. They used ANSYS software for this analysis. Electrochemical shear probe and high-speed camera is used for the measurement of surface shear stress and gas slug rising velocities. They used Plexiglas tube (with a length of 2m and inner diameter of 9.9mm) for data collection of CFD modeling. Here two-phase solution like a mixture of nitrogen gas and electrolyte is used. This literature study conducted 15 experiments with an electrolyte flow rate of 0.1, 0.2, 0.3, 0.4, 0.5 l/min and nitrogen flow rate of 0.1, 0.2, 0.3 l/min. In this CFD model analysis by VOF method. Velocity equation used is given in Equation 2.8,

$$\frac{U_{TB}}{(gd)^{0.5}} = C\frac{u_m}{(gd)^{0.5}} + k \quad (2.8)$$

In CFD model C and k values taken as 1±0.032 and 0.41±0.018 respectively because the flow was in the transition regime range (1300-2800). In buoyancy force simulation, the value of k with 15% deviation is acceptable and for other studies, absolute error less than 10% is acceptable. In this experiment, they use RNG model and concluded that at high liquid and low

gas flow rates the frequency distribution is less than 10% and high gas and low liquid flow case the frequency distribution is greater than 20%.So they used RNG model for turbulent flow and slug flow because these are in transitional regime.

Anthony G. Dixon *et al.* (2011) published a paper about systematic mesh development for 3D CFD simulation. In that they discussed about heat and mass transfer, for heat transfer we want to make finer meshes with high resolution. Here they introduced symmetric approach based on single sphere simulation to mesh full bed particles. They used k–ω SST Reynolds-averaged Navier–Stokes (RANS) for turbulence model with resolved boundary condition and particle drag co-efficient for guiding mesh development. After this study, they found out that Nusselt number is use full for developing boundary layer and near particle meshes.

Kanarska *et al.* (2011) published a paper about Mesoscale simulations of particulate flows with Parallel distributed Lagrange multiplier technique. This study presents, if the computational grid size is high then use two fluids or multi-phase approach. A granular kinetic theory based model is used for representing these two fluids. Empirical two-way coupling relations between fluid and particle were also used in this. If the particle size was large then a combined CFD-DEM coupling approach is used. Motion of individual particle was solved by using Newton's equation of motion. Flow of continuum gas is determined by using CFD. Many verities of continuum fluid codes related with discrete element method (DEM). They used Distributed Legrange multiplier technique for solving particulate suspension flow and these codes uses stationary Eulerian grid. These equations are solved by using fractional step scheme for time discretization. It gave a result free intermediate velocity field without any divergence. The code is parallelized by using SAMRAI frame work.

2.3. OBJECTIVE

Many of the researchers presented experimental and analytical studies about material removal mechanism and current density distribution in ECM using different tool shapes and different software, but they couldn't predict the flow pattern accurately. Passivation is one of the major difficulties in ECM process in the case of complicated shapes. In case of complicated shapes of workpieces, it's very difficult to know the machining variables within the IEG. So there is a need to understand about those parameters (parameters related to flow pattern). Once the flow pattern is known, then it's easy to design the tool and avoid passivation. With this background and the literature review presented in this chapter, the salient objectives of the present study have been identified as follows:

- To optimize the design of L-shaped tool and to study the flow pattern,
- To evaluate the above tool models for efficient machining and determining inlet velocity

2.4. SCOPE OF THE STUDY

In the present work is related to the flow pattern analysis of ECM with four different L shaped tool and studied the various parameters with inlet velocities 36, 43 and 48 m/s.

i. Current density distribution.

ii. Velocity profile.

iii. Temperature pattern.

iv. Turbulence.

v. Shape change of workpiece top surface.

vi. Material Removal Rate (MRR).

2.5. METHODOLOGY

The methodology worked out to achieve the above-mentioned objectives is as follows:

i. Selected L shaped tool for the flow pattern analysis.

ii. As per ECM theory four different designed slots are considered.

iii. Modelled the ECM set up with ANSYS Design Modeller.

iv. The models are Meshed with ANSYS Mesh Module.

v. Analysis this CFD problem with ANSYS CFX.

vi. Observations of results and discussions.

2.6. SUMMARY

This chapter reviews the literature related to ECM and the different modelling and analysis techniques used in there works. The scope and objectives of the study is arrived in this chapter. The methodology used for the present study is number in this chapter.

CHAPTER 3

MODELLING AND ANALYSIS

3.1. INTRODUCTION

This chapter explains the shapes and modeling of the models used for the analysis. The analysis technics and boundary conditions also explained in it. ECM consists of a workpiece, tool and an electrolyte solution. Workpiece should be electrically conducting material and the tool may or may not be. Commonly used electrolytes are NaCl solution and $NaNO_3$. To get required shape in the workpiece tool should design correctly. Tool shape also affects the MRR.

3.2. GEOMETRICAL MODELLING

In the present simulation process four different models are used. The modelling is done with ANSYS Design modeller Module. Those models are named as:

i. Model 1 - L shaped tool with central through hole.
ii. Model 2 - L shaped tool having slot in the tool face with rounded corners.
iii. Model 3 - L shaped model having intermediate chamber and slot in the tool face with rounded corners.
iv. Model 4 - L shaped tool having slot in the tool face with sharp corners.

The initial shape of the workpiece in all models is same. It is circular in shape with 60 mm diameter and 20 mm height. Model of work piece is shown in Figure 3.1. Electrolyte used for this simulation was NaCl solution. It starts flowing from inlet has a constant diameter of 3 mm.

All models are analysed with three different inlet velocities 36 m/s, 43m/s and 48 m/s. These velocities fixed with respect to the flow rate limit (15-20 L/min) of the flow without passivation in the ECM process. Tool outer dimensions are also kept as constant.

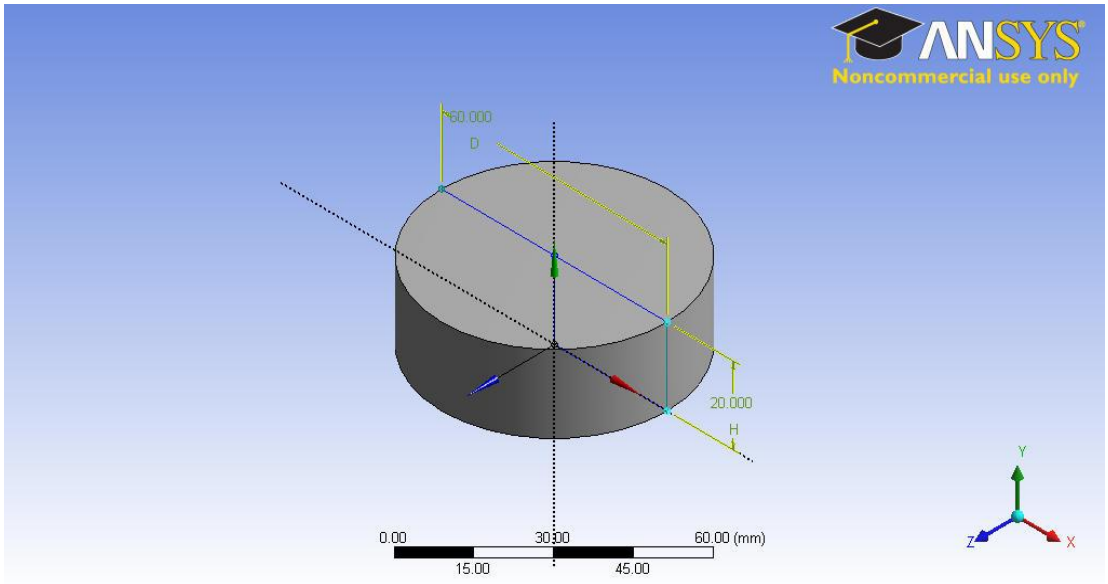

Fig. 3.1: Shape of workpiece used for simulation

Top view of the tool is shown in Figure 3.2. The long side of the L-shape have 30 mm length and short side has 15 mm length and the central hole has diameter 3mm. The only different in these models are the variation in slot arrangement in the face of the tool.

3.2.1. Model 1 – L Shaped Tool With Central Through Hole

Model 1 is a simple L shaped model having a central through hole with a diameter of 3mm and height 50 mm. This centre of the hole is fixed on (-7.5,-7.5) coordinate in the XZ plane. Fluid is flowing through the through hole and flow out through the IEG. Top view of the tool is shown in Figure 3.2 and 3D view is shown in Figure 3.3. Inter electrode gap (IEG) is for all models kept constant is 0.5mm that is shown in Figure 3.4.

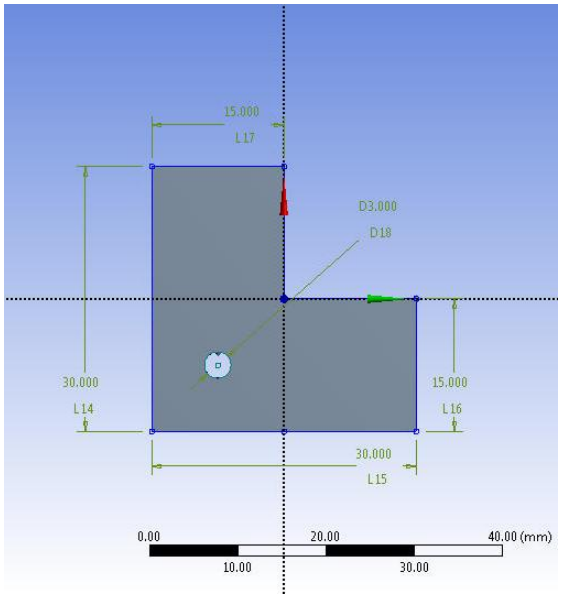

Fig. 3.2: Top view of tool

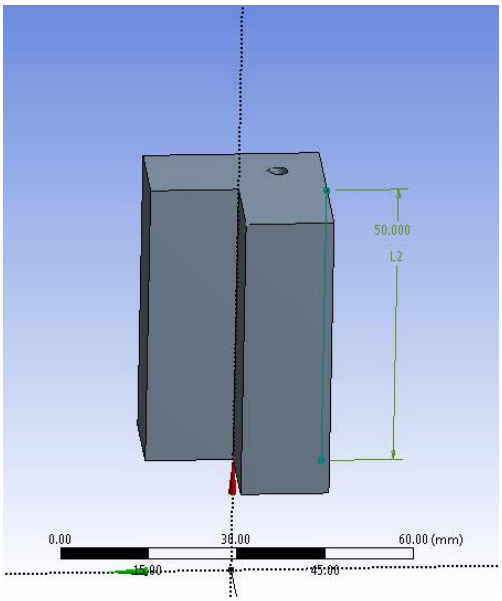

Fig. 3.3: 3D Tool model for Model 1

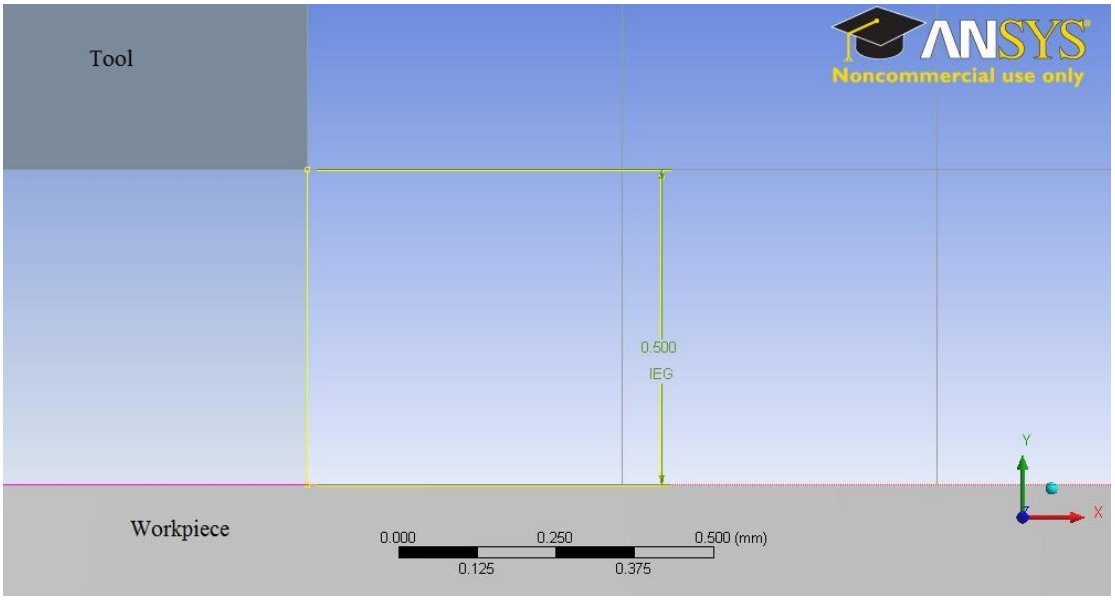

Fig. 3.4: IEG for all models

3.2.2. Model 2- L Shaped Tool Having Slot In The Tool Face With Rounded Corners

Difference of Model 2 from Model 1 is that the bottoms face of the tool having grooves with rounded corners. In this model the central hole have 3 mm diameter and two grooves are connected with this as shown in the Figure 3.4. Those grooves are having a diameter of 0.8 mm and end corners of the grooves with a diameter of 3 mm. Dimensions of this tool is presented in the Figure 3.5. Height of the tool is same as that of previous model. According to tool design for ECM, distance between slot end and corners of workpiece want to keep at least 1.5 mm and the width of the slots are 0.8 mm for best results. These conditions are taken in to account for all tool designs.

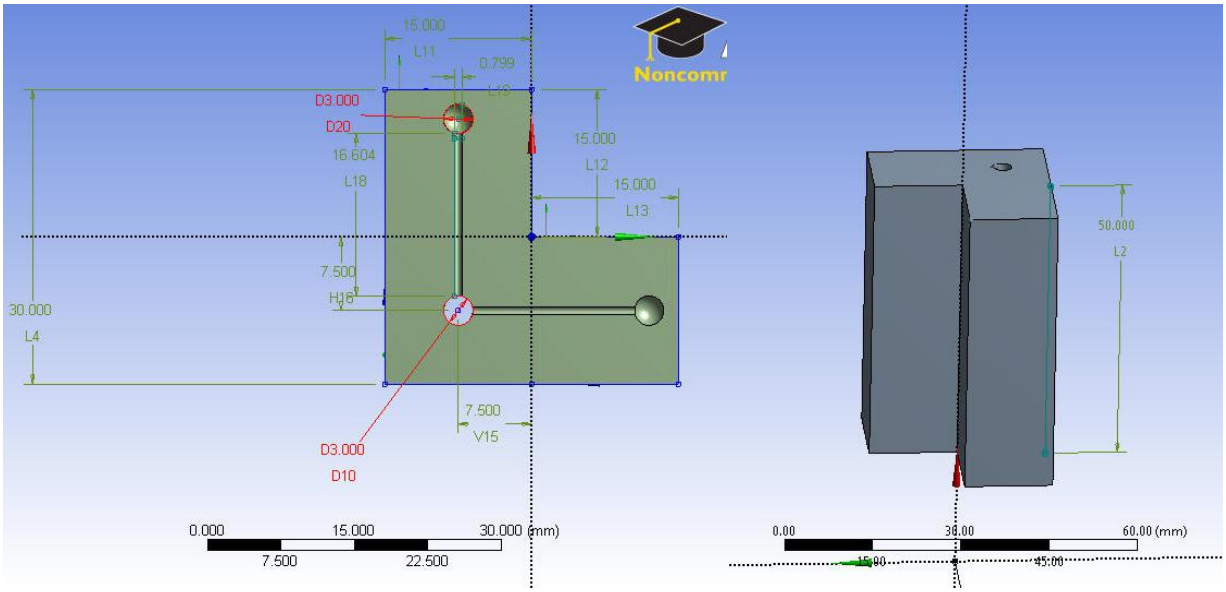

Fig. 3.5: Tool dimensions for Model 2

3.2.3. Model 3 - L Shaped Model Having Intermediate Chamber And Slot In The Tool Face With Rounded Corners.

Model 3 is entirely different from other models. In other models fluid is coming from the inlet and distributed to the grooves at bottom face of the tool. In Model 3 fluid is first come to the L-shaped chamber then it flows to the IEG through slots provided in the bottom of the tool. Here the inlet diameter is given same as like other models but rounded corners in the slot have different dimensions. That design is shown in Figure 3.6. In that slit is in the bottom portion of the chamber. Chamber face dimensions are shown in Figure 3.7 and have a thickness of 1 mm and a height of 5 mm. Chamber constructed for Model 3 is shown in Figure 3.7. Slits in the Model 2 had two rounded end each having a diameter of 3 mm and there is a central rounded portion with a diameter of 5 mm.

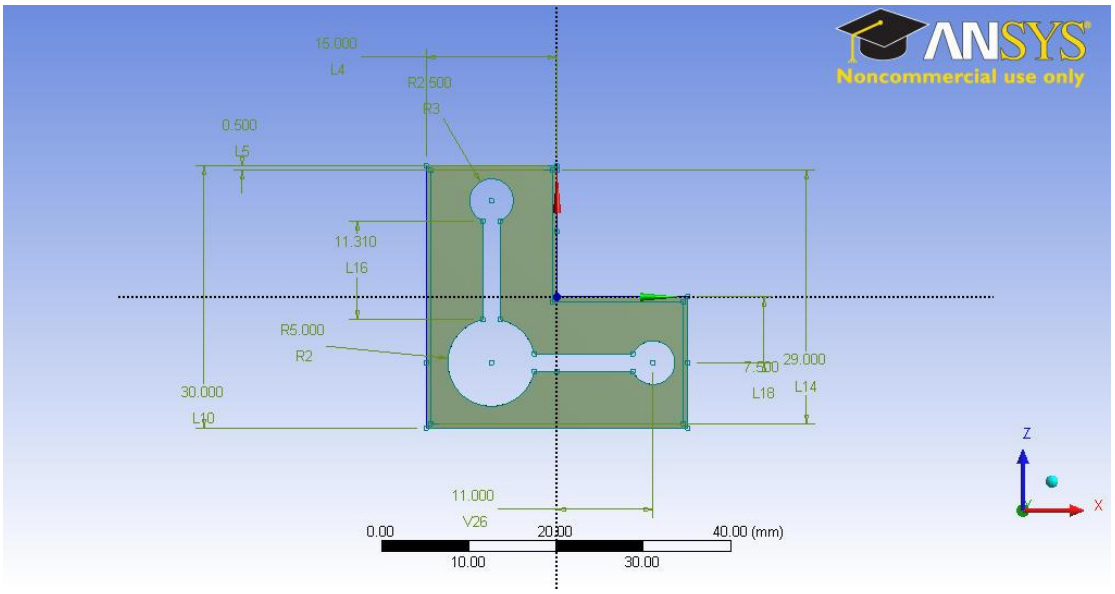

Fig. 3.6: Tool dimensions for Model 3

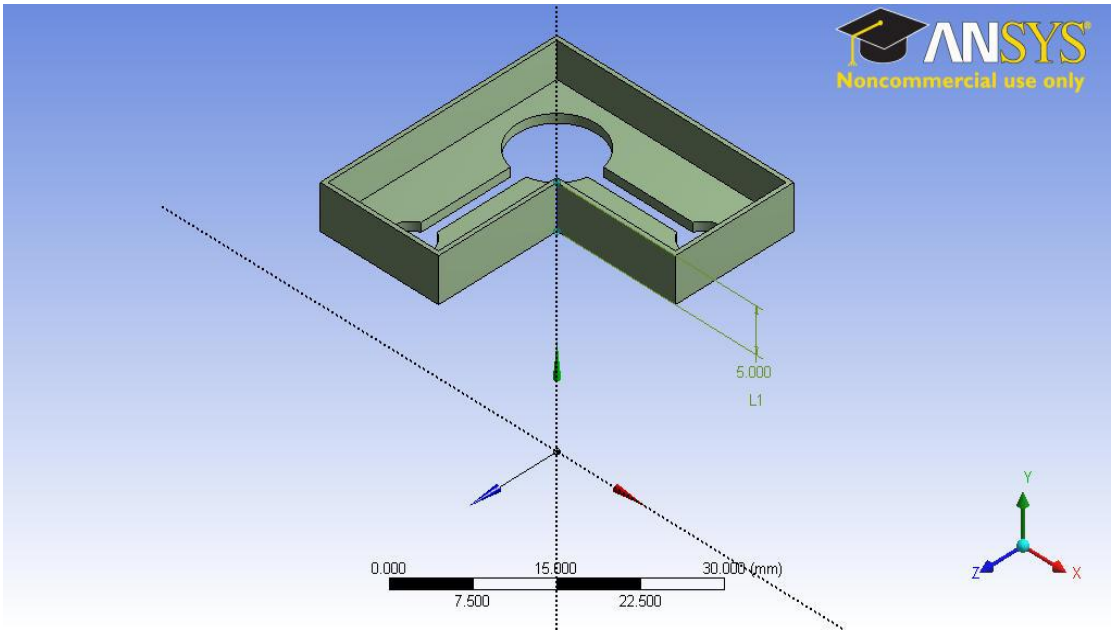

Fig. 3.7: Chamber in the Model 3

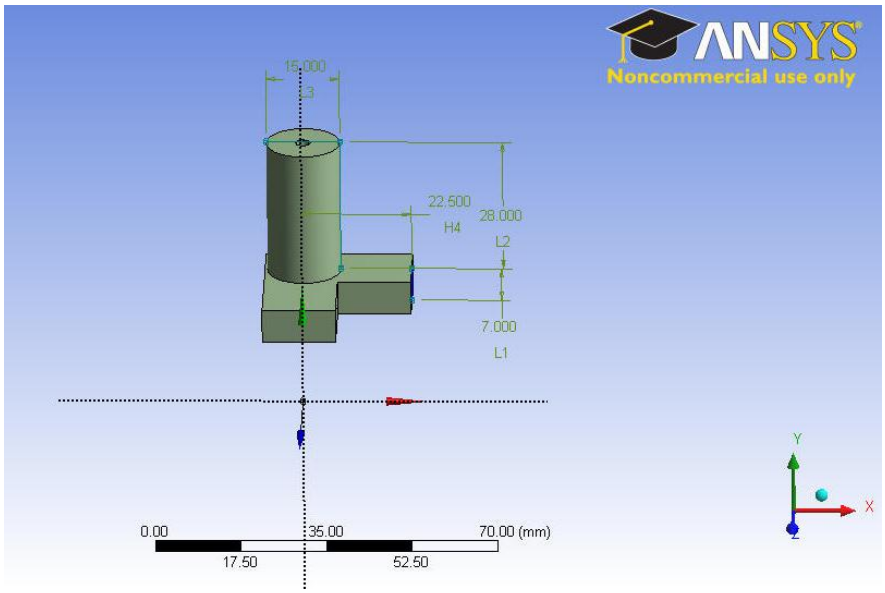

Fig. 3.8: External tool dimensions for Model 3

As per the theory we can gave this diameter up to 6 mm. In this model tool in the inlet portion is hollow cylindrical in shape with an outer diameter 16mm and inner diameter 3 mm. Height of

this hollow cylinder is 28 mm and centre of the hollow cylinder is 22.5 mm from the edge of the L shape. Total outer height of the chamber is 7mm and the elevation dimensions of the tool are shown in Figure 3.8.

3.2.4. Model 4 - L Shaped Tool having Slot in the Tool Face with Sharp Corners

This model is almost same as that of Model 2. The only difference in this model is sharp ended slots. Dimensions of the slots are shown in Figure 3.9. It consists of a small circular end with a diameter 0.8 mm and height of 50 mm.

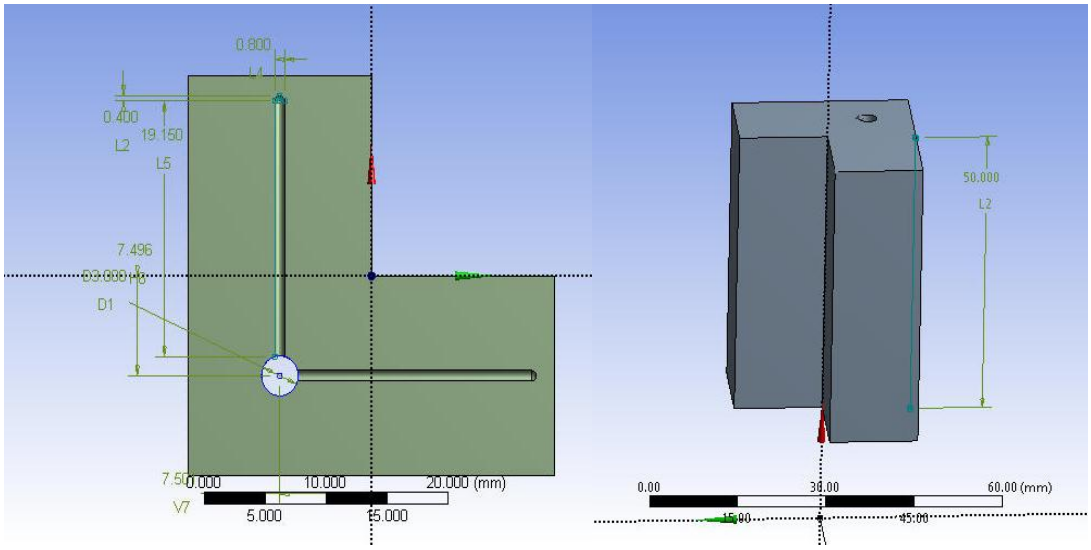

Fig. 3.9: Tool dimensions for Model 4

3.3. MESHING

Models are meshed using ANSYS Mesh Module in ANSYS commercial software. The quality of mesh is relevant in the case of model geometry and results accuracy. This can be expressed with orthogonal quality, if it is coming near to '1' then our mesh quality is good and it gives better

results. Same time if it is coming near to zero that meshes give bad results. Tetrahedral elements are used for meshing these geometries and elements have a minimum edge length 5×10^{-4} m. Tetrahedral meshes generally provides more automatic solutions with ability to add mesh controls to improve accuracy in critical region. Hexahedral meshes generally give more accurate results but it's very difficult to generate. Program controlled automatic inflation method is enabled for meshing. Mesh methods included in ANSYS are Patch conforming and Patch independent methods. Out of that Patch independent meshing method is adopted for meshing present model geometries. Patch independent method uses top down approach that means it creates volume mesh and extracts surface mesh from boundaries. Advantages of this method are it uses the geometry only to associate the boundary faces of the mesh to the region of interest there by ignoring gaps, overlaps and other issues that present in other meshing tools. Sections in the model are named as specified below.

i. Tool

Tool top – Top face surface of tool

Tool bottom surface – bottom face surface of tool

Tool groove – Hollow surface in the tool

Tool outer – Outer surfaces of tool

ii. Workpiece

Work top - Top face surface of workpiece

Work bottom - Bottom face surface of workpiece

Work outer – Outer surfaces of workpiece

iii. Brine (Electrolyte)

Velocity inlet – Starting region of electrolyte

Pressure outlet – The portion which electrolyte is flowing out

Brine groove – It is the portion of electrolyte inside the tool groove

Brine bottom - Bottom face of brine which making contact with

Brine top - Top face of brine which making contact with tool bottom.

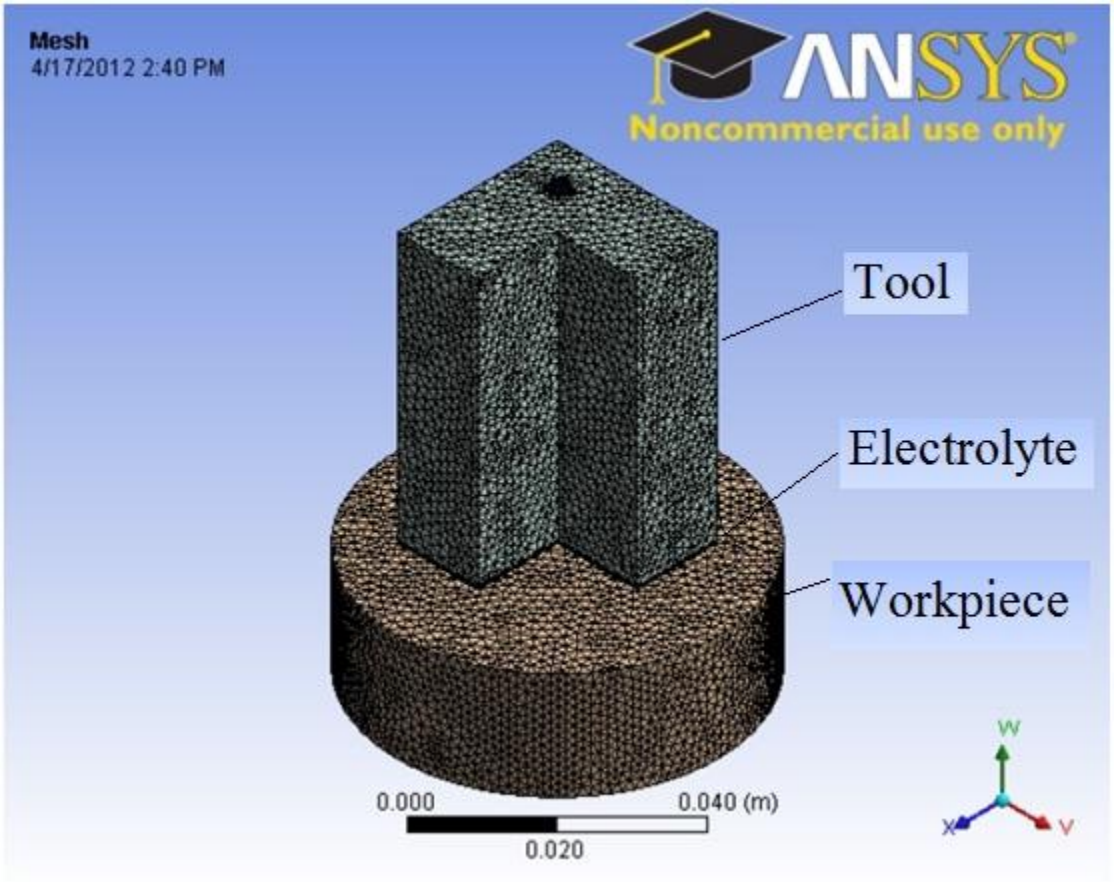

Fig. 3.10: Outer shape of meshed model for Models 1, 2 and 4.

Table 3.1: Meshing properties for all models generated

Model No.	Nodes	Elements	Skewness	Orthogonal quality
Model 1	3320377	2392617	0.640137	0.9878
Model 2	341842	625685	0.893000	0.9960
Model 3	500050	2597095	0.840000	0.9994
Model 4	344130	637849	0.860000	0.9980

Meshed model used for these analyses is given in the Figure 3.10.Meshing details for all models are explained in the table 3.1.

3.4. GOVERNING EQUATIONS

Simulations are based on governing equations are mainly two types, first one is Computational Fluid Dynamic model equations and other is some user defined equations used for modelling. Fist kind is inbuilt in the software model ANSYS and second is the defined by the user.

3.4.1. Computational Fluid Dynamic Model Equations

Reynolds no in the inlet itself is more than 4000 that means flow is in the turbulent region. So we want to enable a turbulent model for this simulation. Here k-ε model is used for solving this problem. This model is a two equation model. It uses gradient based hypothesis for making relation between Reynolds stress to the mean velocity gradient and the turbulent viscosity. In that 'k' is the turbulent kinetic energy expressed as the variance of fluctuations in velocity. Unit of

'k' is m^2/s^2. 'ε' is the rate at which the velocity fluctuations dissipate, it is called as turbulent eddy dissipation. Unit of 'ε' is m^2/s^3. Equation 3.1 is the continuity equation and Equation 3.2 is the momentum equations for these models.

$$\frac{\partial \rho}{\partial t} + \frac{\partial}{\partial x_j}(\rho u_j) = 0 \tag{3.1}$$

$$\frac{\partial \rho u_i}{\partial t} + \frac{\partial}{\partial x_j}(\rho u_i u_j) = \frac{\partial P'}{\partial x_i} + \frac{\partial}{\partial x_j}\left(\mu_{eff}\left[\frac{\partial u_i}{\partial x_j} + \frac{\partial u_j}{\partial x_i}\right]\right) + S_m \tag{3.2}$$

$$\mu_{eff} = \mu + \mu_t \tag{3.3}$$

The k-ε model is assumed as the turbulent viscosity is depends on turbulent kinetic energy and dissipation. That relation is shown in equation 3.4.

$$\mu_t = C_\mu \rho \frac{k^2}{\varepsilon} \tag{3.4}$$

k and ε values are coming directly from the differential equations for turbulent kinetic energy and dissipation rate. Those equations are given in Equations 3.5 and 3.6.

$$\frac{\partial(\rho k)}{\partial t} + \frac{\partial}{\partial x_j}(\rho u_{jk}) = \frac{\partial}{\partial x_j}\left[(\mu + \frac{\mu_t}{\sigma_k})\frac{\partial k}{\partial x_j}\right] + P_k - \rho_\varepsilon + P_{kb} \tag{3.5}$$

And

$$\frac{\partial(\rho \varepsilon)}{\partial t} + \frac{\partial}{\partial x_j}(\rho u_j \epsilon) = \frac{\partial}{\partial x_j}\left[(\mu + \frac{\mu_t}{\sigma_\epsilon})\frac{\partial \epsilon}{\partial x_j}\right] + \frac{\varepsilon}{k}[C_{\varepsilon 1} P_k - C_{\varepsilon 2}\rho_\varepsilon + C_{\varepsilon 1} P_{\varepsilon b}\,] \tag{3.6}$$

Value for P_k is getting from the relation given in Equation 3.7.

$$P_k = \mu_t \left(\frac{\partial u_i}{\partial x_j} + \frac{\partial u_j}{\partial x_i} \right) \frac{\partial u_i}{\partial x_j} \quad (3.7)$$

It consists of one more term but in our problem effect of that term is less. So we can neglect that term because for incompressible flow ($\frac{\partial u_k}{\partial x_k}$) having less effect. It has effect in compressible flow with high velocity divergence.

For making heat transfer model constructed the solid domains as conjugate heat transfer (CHT) domains. In CFX, boundaries between domains that model heat transfer have temperatures and thermal fluxes calculated automatically and should not have to specify the thermal boundary conditions. Source of thermal energy and /or radiation can also be added to a CHT domain. ANSYS CFX allow to create solid regions in which the equations for heat transfer are solved, but without flow. This is known as conjugate heat transfer. Inside the solid domains conservation of energy equation is simplified since there is no flow inside the solid, thus conduction is the only mode of heat transfer. The heat conduction through the solid has transport equations as like shown in Equation 3.8.

$$\frac{\partial \rho \, C_p T}{\partial t} = \nabla . (k \nabla T) + S_E \quad (3.8)$$

3.4.2. User Defined Equations

For finding out the velocities the know thing is volume flow rate range for the electrolyte. Using continuity equation shown in the Equation 3.9 it is ease to found the inlet velocities within that range. The inlet velocity is kept constant for that purpose. Value for the inlet velocity is 3 mm/s.

$$Q = Av \tag{3.9}$$

Deformation of each node can calculate from Faraday's law presented as Equation 3.10.

$$\Delta d = \frac{\epsilon A J \Delta t}{\rho z F} \tag{3.10}$$

In Equation 3.10 current density (J) is changing according to the conductivity. Current density is obtained from the Equation 3.11.

$$J = \frac{k(V - \Delta V)}{y} \tag{3.11}$$

From the above relation it is understand that current density depends up on thermal conductivity (k) and inter electrode gap (IEG). But in this simulation process y is kept constant as 0.5mm. Thermal conductivity is proportional to the temperature as shown in the Equation 3.12.

$$k = k_0(1 + \alpha(T_b - T)) \tag{3.12}$$

Volume of the removed region in the workpiece is calculated from the Equation 3.13. In this relation 'h' is the height of the deformed nodes from the top surface of the workpiece. That is equal to the deformation of nodes Δd. Value of area is getting from the Equation 3.14.

$$V_r = \left(\sum_{1}^{N} ah\right)/t \tag{3.13}$$

$$a = \sqrt{3}\, l^2 \tag{3.14}$$

3.5. MATERIAL PROPERTIES

Materials used for making this simulation are, Iron as workpiece, Copper as tool and 20% brine solutions as electrolyte. Data's for this simulations are taken from reference [17] and [18]. Material properties are given in Table 3.2.

Table 3.2: Material Properties

Properties	Brine	Copper	Iron	Air
Molar mass(Kg/Kmol)	58.44	63.55	55.85	-
Density(Kg/m^3)	1050	8933	7860	-
Specific heat(j/KgK)	3760	385	460	-
Dynamic viscosity(Pa s)	0.001	-	-	-
Thermal Conductivity(W/mK)	0.6	401	80	-
Electrical Conductivity(S/m)	8.43	5.96E+07	1E+07	-
Convection coefficient (W/m^2K)	1000	-	-	100

3.6. ANALYSIS

This analysis done in ANSYS CFX software because it is simpler than FLUENT and MHD option can easily enable within this software. For doing this analysis firstly we need to set the analysis as steady or transient state. These simulations are set it as steady state problem.

3.6.1. Assumptions

As like every simulations for this simulation also assuming some assumptions. Those assumptions are,

i. The inter electrode gap is constant.

ii. Material property of the tool and workpiece never change throughout the analysis.

iii. Tool and workpiece material are homogeneous.

iv. Heat generation is due to Joule's heating.

v. The electrolyte is in liquid state and no H_2 gas is evolved

vi. Material removal only depends on current density

3.6.2. Boundary Conditions

The computational domains should specify first before specifying the boundary conditions. In this simulation three domains are used. Two solid domains and a fluid domain, one solid domain for workpiece and other is for tool. Solid domain materials are in the material group conjugate heat transfer solids and consider as pure solids. Morphology of material is given as continuous solid and reference temperature is given 300K. Electric potential model with automatic value is chosen from Electromagnetic model. Fluid domain is constructed for electrolyte. Morphology for fluid domain is taken as continuous fluid. Material properties are given in the Table 3.1. Only the conductivity of electrolyte is varying with respect to temperature according to the equation 3.14 other values are kept constant. This equation is written as CEL expression and directly assigned it as material property. α- value is taken as 0.02 for brine and boiling temperature for brine is taken as 373K. Valence for iron is taken as 2. In this simulations Iron is used as

workpiece material, copper is used as tool material and brine solution is used as electrolyte. Same boundary conditions are given for all models that are given according to Annexure A. Boundary conditions used for these simulations are given below,

i. Inlet

Mass and Momentum = Normal speed = 36, 43 and 48 m/s

Flow regime = Subsonic

Turbulence = Given intensity and auto computation length

Fractional intensity =0.06

Heat transfer static temperature = 300K

Electric field = 0 flux

ii. Outlet

Mass and Momentum = Opening pressure and direction = 0 Pa and flow normal to the boundary

Flow regime = Subsonic

Turbulence = Given intensity and auto computation length

Fractional intensity =0.06

iii. Tool

a. Tool Top

Heat transfer = Convection

Convection heat transfer coefficient = $100 W/m^2 K$

Electrical potential = Voltage

= 0 V

b. Tool Outer

Heat transfer = Convection

Convection heat transfer coefficient = 100W/m^2 K

iv. Workpiece

a. Work Bottom

Heat transfer = Convection

Convection heat transfer coefficient = 100W/m^2 K

Electric field = Voltage

= 10 V

b. Work Outer

Heat transfer = Convection

Convection heat transfer coefficient = 100W/m^2 K

v. Interface

a. Brine Tool

It is the interface between brine top and tool bottom. Type of interaction used for this is Fluid-Solid.

Heat transfer = Thin material

Heat transfer in Copper = 0.05 m.

GGI type mesh connection is used to connect meshes.

b. Brine Work

It is the interface between brine bottom and workpiece top.

Heat transfer = Thin material

Heat transfer in Iron = 0.02 m

GGI type mesh connection is used to connect meshes.

After boundary conditions set up we need to manage the solver control. High resolution is taken for advection scheme. High resolution is given for turbulence numeric. 1 and 300/600 are given as minimum and maximum time step respectively. Maximum value time step is set 300 or 600 because in some simulation are carried out with both 30s and 60s. Fluid time scale control is set as physical time scale, in that time scale value is given as 0.1s. In that this simulations done as an iterative process so first want to set convergence criteria. Root Mean Square (RMS) value 1×10^{-5} is set as convergence criteria. Run mode is selected as HP MPI distributed parallel.

After completion of these analyses, took out the value of current density of workpiece at each node in the *csv* format for calculating the deformation. Calculate deformation in each and every node within the workpiece with an electric potential more than 1.5V using the equation 3.12. Deduct this value from Y value and call back the result file in to CFD post. From that file it possible to get the deformed shape of the workpiece. The value of MRR was found by using the Equation 3.15. In that value of 'a' is the edge length of tetrahedron. In place of *'t'* put the value 30 or 60 according to the model.

3.7. SUMMARY

The geometry of different model is explained with figures to support that. The meshing of the models also explained in this chapter. The basic theory behind the CFX used by the ANSYS software also is explained in it. The governing equations supporting the simulation and some user defined equations also presented in it. The material properties of tool, workpiece and electrolyte are presented in the Table 3.2. The specification of ECM machine is shown in the Table 3.3. The analysis method with assumptions and boundary conditions used are presented in this chapter.

CHAPTER 4

RESULTS AND DISCUSSIONS

4.1. INTRODUCTION

In this chapter, the parameters effecting ECM process are explained with the help of charts and graphs. These velocity, current density, turbulent kinetic energy, turbulent eddy dissipation, shape change of work piece and MRR with respect to inlet velocity are discussed for the four different models generated using the commercial software ANSYS.

4.2. EFFECT ON VELOCITY PROFILE

Figs. 4.1, 4.2, 4.3 and 4.4 are the velocity profiles within the IEG of the models (Model 1, 2, 3 and 4) used for the stimulation. The velocity profiles are plotted for the range = 0 to 30 m/s for the present study of the specimens.

In Fig. 4.1, the velocity is approximately 30 m/s near the central through hole. The surrounding of the central through hole has a small variation of velocity due to stagnation. That means the incoming electrolyte with high velocity first makes contact with the workpiece where it releases most of the kinetic energy that region is called stagnation region and the velocity is called stagnation velocity. After that, the velocity is decreasing smoothly, but it is less than 5 m/s in some region towards the tip of the tool (shown in Fig. 4.1 with blue colour). According to ECM theory, passivation occurs due to deposition of sludge on the workpiece and tool surfaces because of insufficiency flow of electrolyte within the IEG. If velocity less than 5 m/s, then it is more likely to the surface will passivate and prevent further machining. From Fig. 4.1, it's clear that there is passivated area within the model.

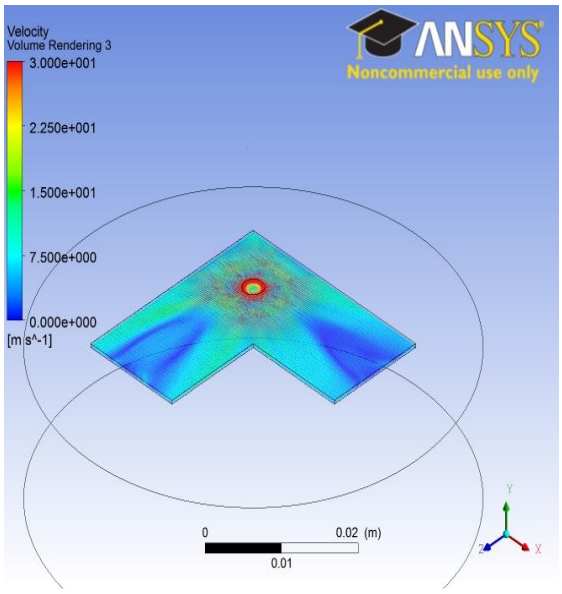

Fig. 4.1: Velocity profile of Model 1 with an inlet velocity 36m/s.

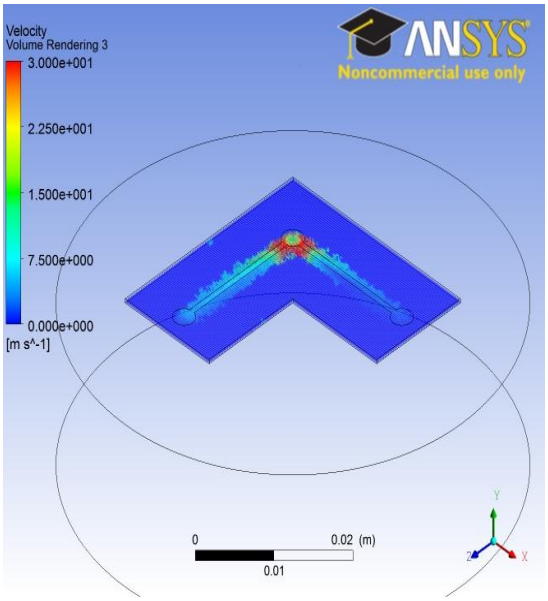

Fig. 4.2: Velocity profile of Model 2 with an inlet velocity 36m/s.

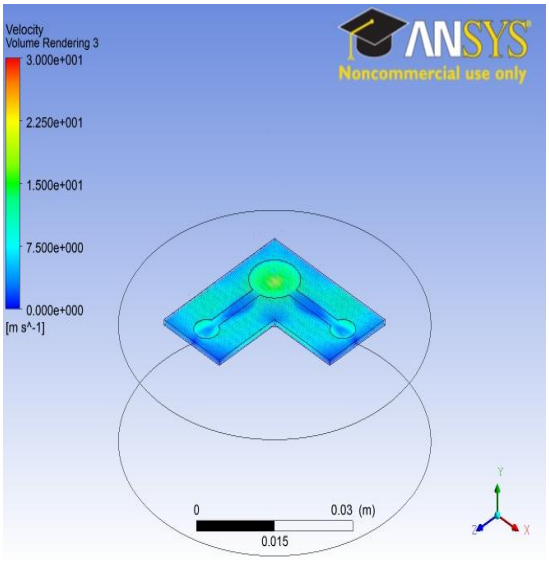

Fig. 4.3: Velocity profile of Model 3 with an inlet velocity 36m/s.

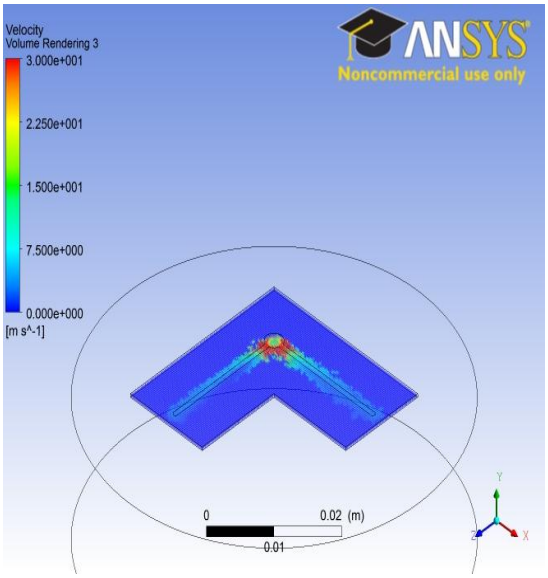

Fig. 4.4: Velocity profile of Model 4 with an inlet velocity 36m/s.

In Model 2, the velocity near the groove is more than 5 m/s and in all other region it fall below 5 m/s, that means other areas will get passivated. In case of Model 3, from Fig. 4.3, it can be

easily understood that the velocity variation is smooth and a small region is having velocity < 5 m/s. Here stagnation effect is less because first the electrolyte entering in to a small chamber and then it coming out through the grooves. The velocity profile in Model 4 is similar to Model 2 which means that except near the grooves all other areas will get passivated.

Among these four models, Model 3 is the best in the sense of velocity profile. Hence, extended simulation of Model 3 with higher velocities was conducted. The velocity distributions are shown in Fig. 4.5 and 4.6 for inlet velocity = 43 and 48 m/s, respectively. From these figures, it can be concluded that passivation tendency decreasing with increasing inlet velocity.

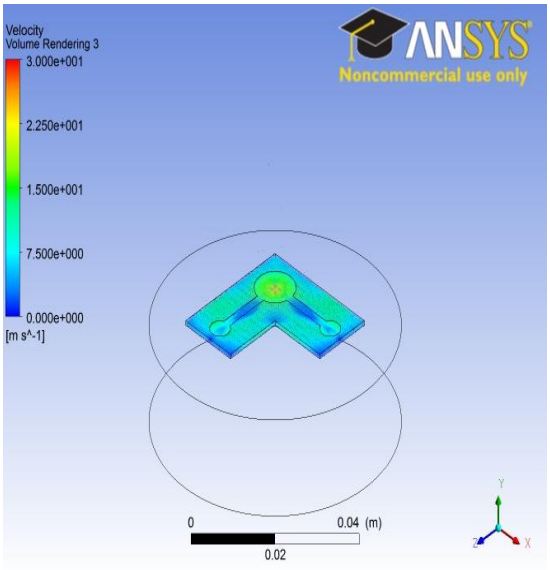

Fig. 4.5: Velocity profile of Model 3 with an inlet velocity 43m/s.

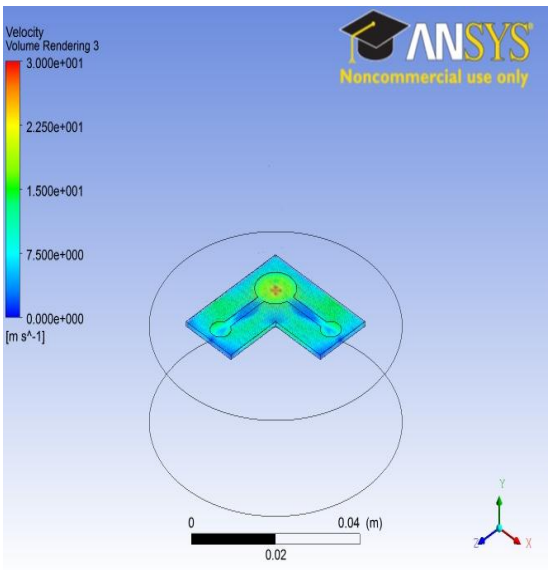

Fig. 4.6: Velocity profile of Model 3 with an inlet velocity 48m/s.

4.3. EFFECT ON STREAM LINE

The streamlines are generally representing the velocity flow pattern in a fluid flow. Figs. 4.7, 4.8, 4.9 and 4.10, are the bottom view of the 3D streamline pattern for Model 1, 2, 3 and 4, respectively.

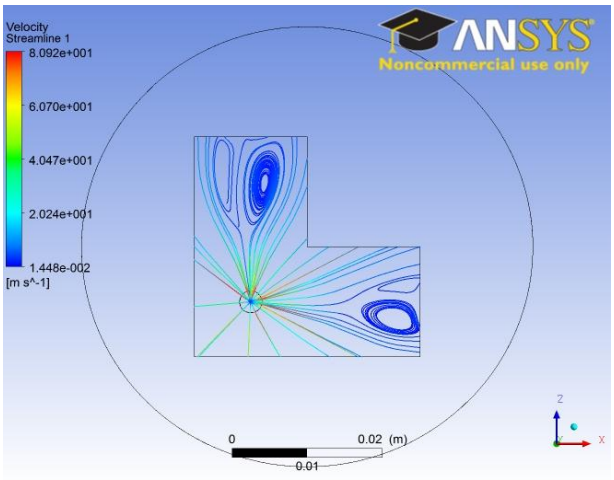

Fig. 4.7: Streamline flow of Model 1 with an inlet velocity 36m/s

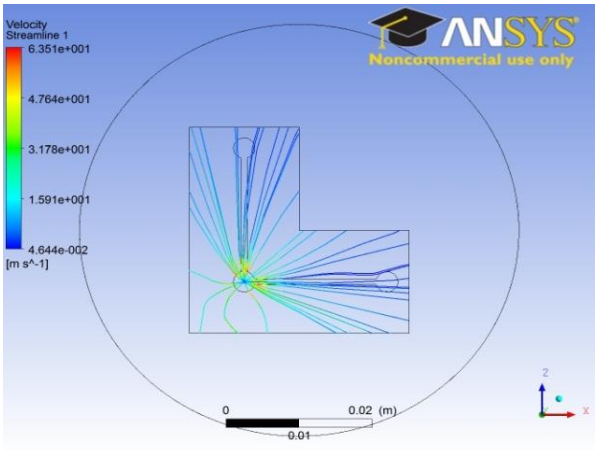

Fig. 4.8: Streamline flow of Model 2 with an inlet velocity 36m/s

From Fig. 4.7, it can be understood that there is eddy formation in the flow pattern in the end region of the 'L' and velocity in the eddy region is less than 5m/s. In Fig. 4.8 and 4.10, the streamlines are almost similar to each other. These defects cause passivation within the IEG. In Fig. 4.9, for Model 3, the streamlines are distributed in proper manner. The end of the groove the streamline arrangement is ambiguous in nature, so it needs some more clarification. From the inset figure, it is evident that the flow is from top upper chamber to bottom in IEG and it gets distributed throughout. From the above figures, it can be understood that Model 3 is the best, so we continue the simulation of Model 3 with increasing inlet velocities 43 m/s and 48 m/s. Those

results are shown in Fig. 4.11 and 4.12. In these plots, the distributions of streamlines are also satisfactory.

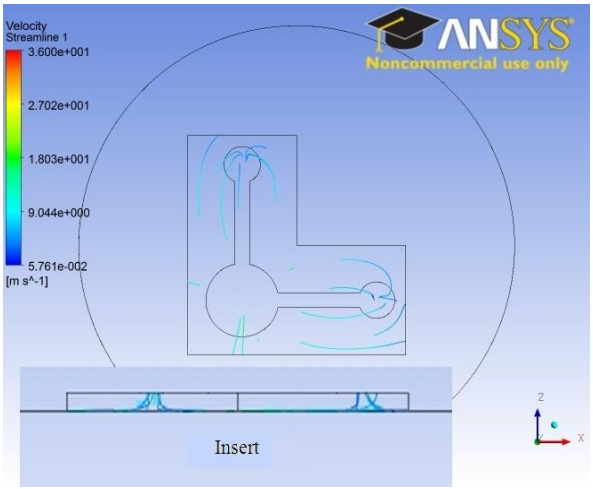

Fig. 4.9: Streamline flow of Model 3 with an inlet velocity 36m/s

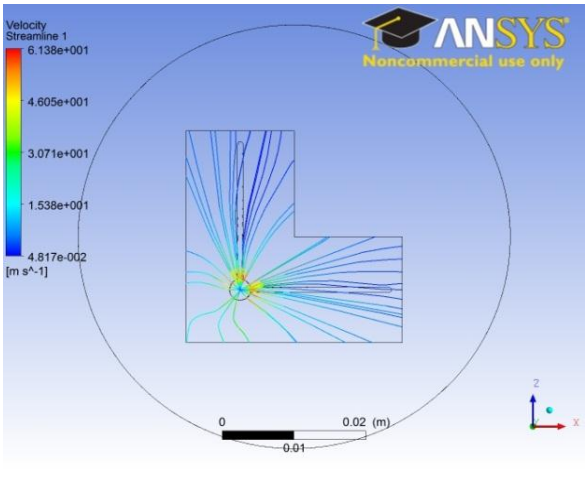

Fig. 4.10: Streamline flow of Model 4 with an inlet velocity 36m/s

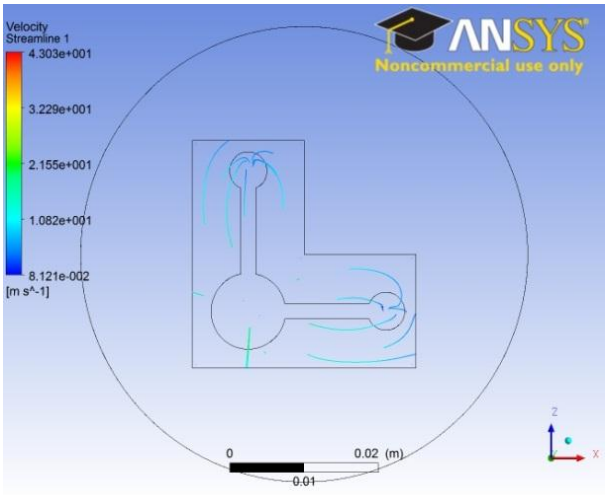

Fig. 4.11: Streamline flow of Model 3 with an inlet velocity 43 m/s

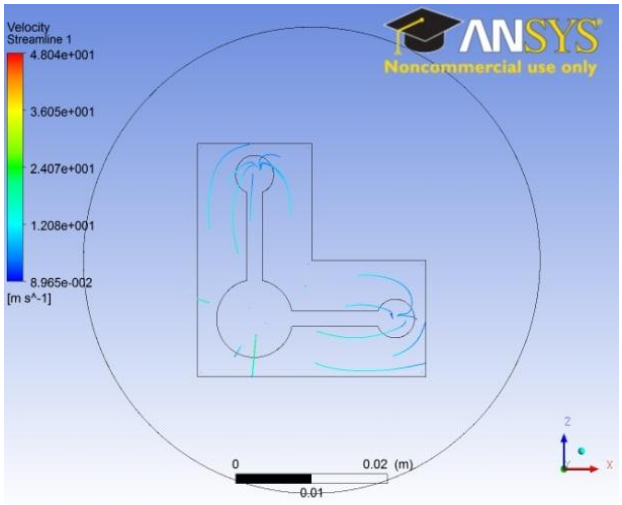

Fig. 4.12: Streamline flow of Model 3 with an inlet velocity 48 m/s

4.4. EFFECT ON TURBULENT KINETIC ENERGY (k)

Figs. 4.13, 4.14, 4.15 and 4.16 are the turbulence kinetic energy within the IEG for Models 1, 2, 3 and 4, respectively, with an inlet velocity 36 m/s. Turbulence in the k- ε model is depends on turbulent kinetic energy (k) and turbulent eddy dissipation (ε). If the turbulence within the IEG is more, then it means that roughness of the machined surface will be more. Turbulent kinetic energy determines the energy in the turbulence. Turbulent kinetic energy produced by fluid shear, friction or buoyancy or through external forcing at low frequency eddy scale.

In model 1, near the central through hole turbulent kinetic energy is less due to stagnation. The surrounding of the central through hole has a large variation of turbulent kinetic energy. That is because of sudden buildup of high pressure in the stagnation region. After that region 'k' value is coming to minimum value range. The 'k' value for Model 1 varies from 3.759×10^{-2} to 1.102×10^{1} m^2/s^2. In Model 2, 'k' value is less than that of Model 1, and it varies from 9.263×10^{-3} to 0.7469×10^{1} m^2/s^2. The 'k' value is less than the above two models for Model 3, so this will give better machining surfaces. It varies from 2.343×10^{-3} to 0.2829×10^{1} m^2/s^2. For Model 4, the `k' value varies from 3.972×10^{-2} to 1.365×10^{1} m^2/s^2, which indicate that in Model 4 the effect of turbulence is more than in Model 3.

Fig. 4.17 is the chart plotted variations of log value of turbulent kinetic energy in the Brine solution within the IEG versus the four models. The range of values of 'k' is less in the case of Model 1 but the minimum and maximum values are more than Model 3. In case of Model 4 and 2, they are also higher values than that of Model 3. It can be understood that Model 3 is the best among those models in the sense of turbulent kinetic energy because of the maximum and minimum 'k' values are less.

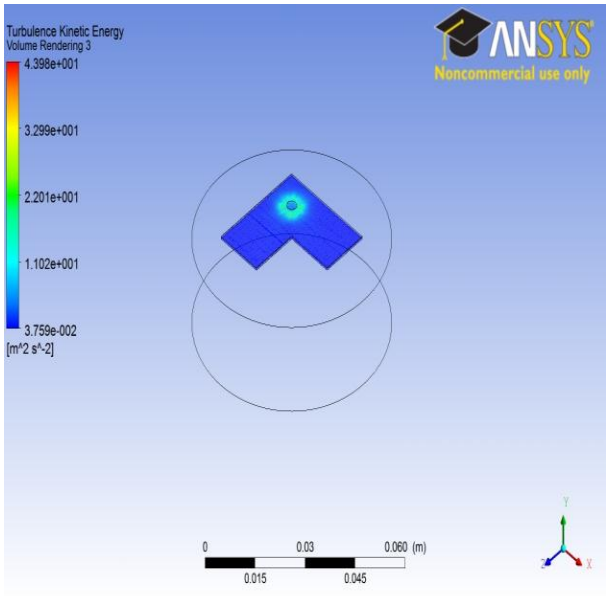

Fig. 4.13: Turbulent Kinetic energy of Model 1 with an inlet velocity 36m/s.

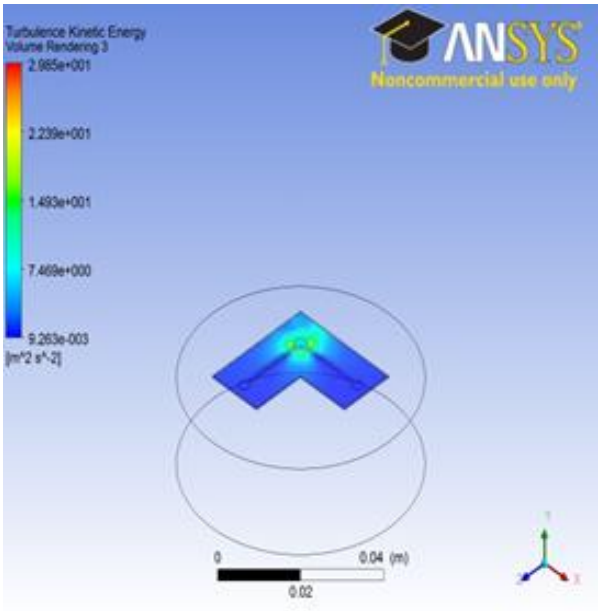

Fig. 4.14: Turbulent Kinetic energy of Model 2 with an inlet velocity 36m/s

We continue the simulation of Model 3 with increasing inlet velocities 43 m/s and 48 m/s and the results are shown in Fig. 4.18 and 4.19. As per theory, increase in velocity will create more turbulence in the flow. The Turbulent kinetic energy values vary in the range of 2.898×10^{-3} m^2/s^2 to $3.831 m^2/s^2$ and 3.427×10^{-3} m^2/s^2 to 4.624 m^2/s^2 with inlet velocity 43 and 48 m/s, respectively. The turbulence KE is much less for Model 3 with higher inlet velocities when compared with other three models.

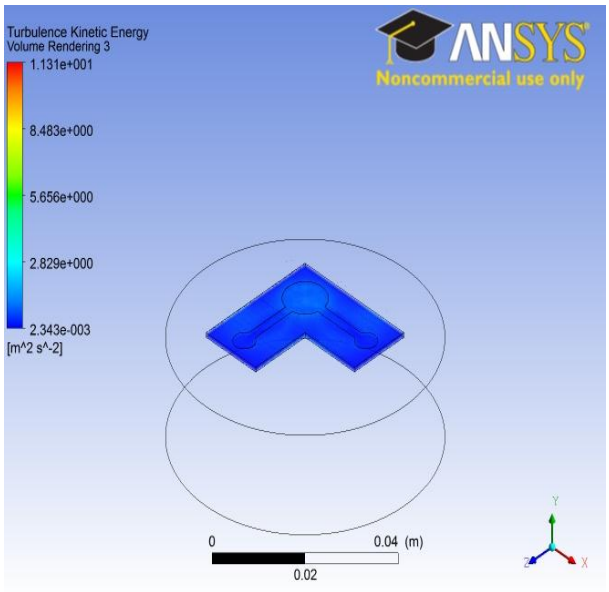

Fig. 4.15: Turbulent Kinetic energy of Model 3 with an inlet velocity 36m/s

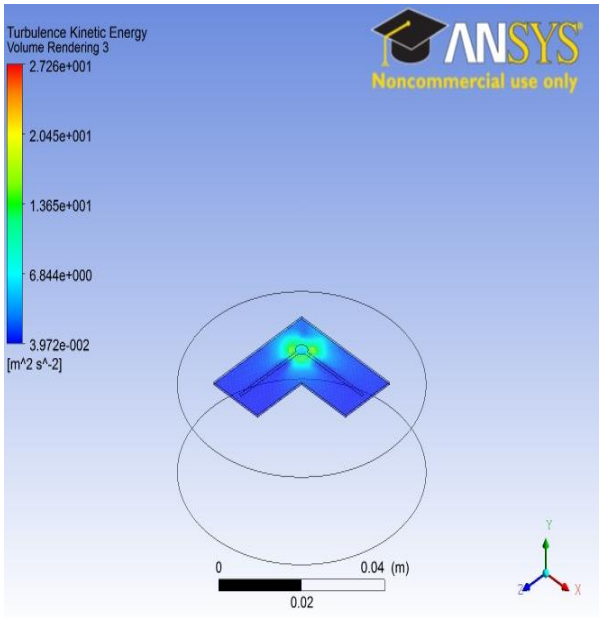

Fig. 4.16: Turbulent Kinetic energy of Model 4 with an inlet velocity 36m/s

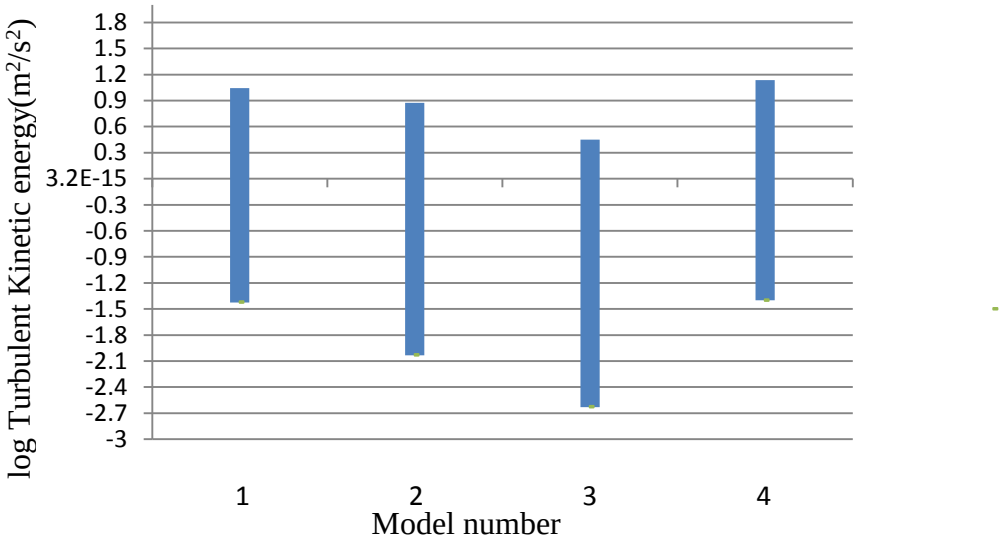

Fig. 4.17: Turbulent Kinetic energy variations of all the four Models with an inlet velocity 36 m/s

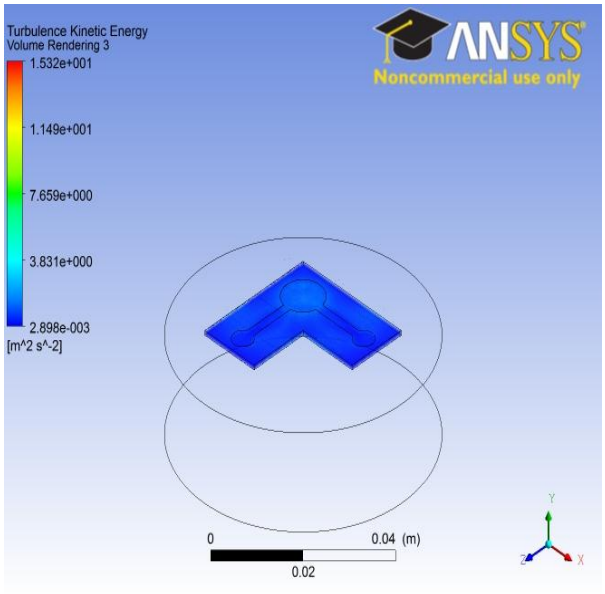

Fig. 4.18: Turbulent Kinetic energy of Model 3 with an inlet velocity 43m/s.

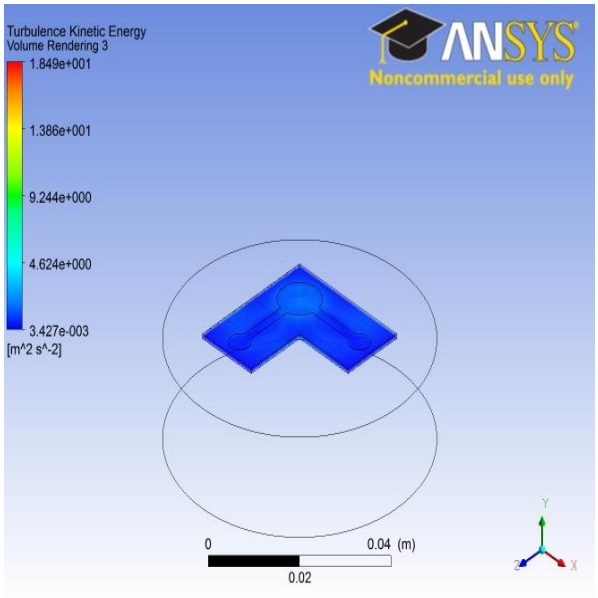

Fig. 4.19: Turbulent Kinetic energy of Model 3 with an inlet velocity 48m/s.

4.5. EFFECT ON TURBULENT EDDY DISSIPATION

Turbulent eddy dissipation (ε) determines the scale of turbulence. Figs. 4.20, 4.21, 4.22 and 4.23 are the turbulence eddy dissipation within the IEG for Models 1, 2, 3 and 4, respectively, with an inlet velocity 36 m/s. In model 1, near the central through hole turbulent eddy dissipation is less due to stagnation. The surrounding of the central through hole has a large variation of turbulent eddy dissipation hereafter there is no change in ε. In Model 1, the turbulence eddy dissipation values ranges from 2.972×10^{2} m^2/s^3 to 3.394×10^{6} m^2/s^3. Here the distributions of 'ε' values are in circular form because of central hole.

In case of Model 2, the variation of 'ε' distribution is more than that of Model 1 and it is not circular in shape because of groove effect and the 'ε' values are ranges from 1.249×10^{2} $m^2/s^3$to

1.045×10^{6} m^2/s^3, which is less than that of Model 1. In Model 3, the 'ε' values are varies from 3.488×10^{-1} m^2/s^3 to 1.2×10^{5} m^2/s^3, which is much lesser than that of other models. In Model 4, the 'ε' values are varies from 1.553×10^{2} to 8.852×10^{5} m^2/s^3. This value is greater than that of Model 3 and less than that of Model 1 and 2.

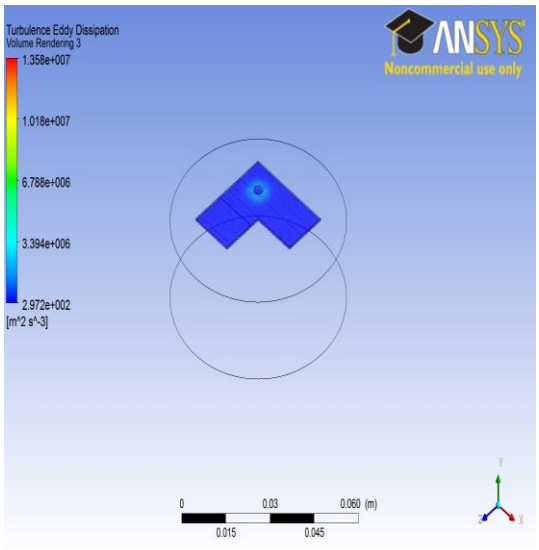

Fig. 4.20: Turbulence Eddy Dissipation of Model 1 with an inlet velocity 36m/s.

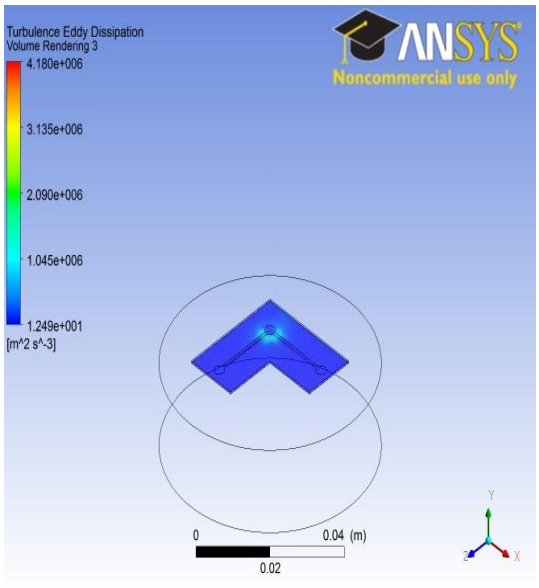

Fig. 4.21: Turbulence Eddy Dissipation of Model 2 with an inlet velocity 36m/s.

Fig. 4.24 is the chart plotted variations of log value of turbulent eddy dissipation in the Brine solution within the IEG versus the four models. The ε value range is less in case of Model 3. In other models, the maximum and minimum values are more than that of Model 3. From the above discussion, it can be understand that Model 3 is the best, so we continue the simulation of Model 3 with increasing inlet velocities 43 m/s and 48 m/s. Those results are shown in Fig. 4.25 and 4.26. That value ranges from 5.662×10^{-1} m^2/s^3 to 1.894×10^{5} m^2/s^3 and 7.869×10^{-1} m^2/s^3 to 2.513×10^{5} m^2/s^3, respectively. That we know that if velocity increases turbulence is also

increases. When compared to Model 3 with inlet velocity 36 m/s, these results showing more 'ε' value and the same had less value than that of other three models.

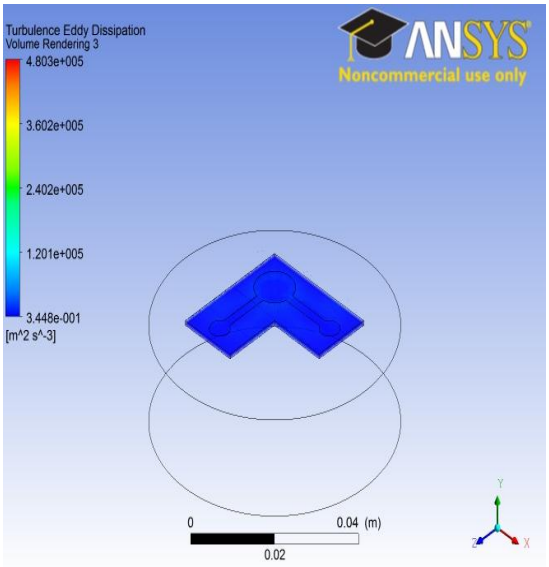

Fig. 4.22: Turbulence Eddy Dissipation of Model 3 with an inlet velocity 36m/s.

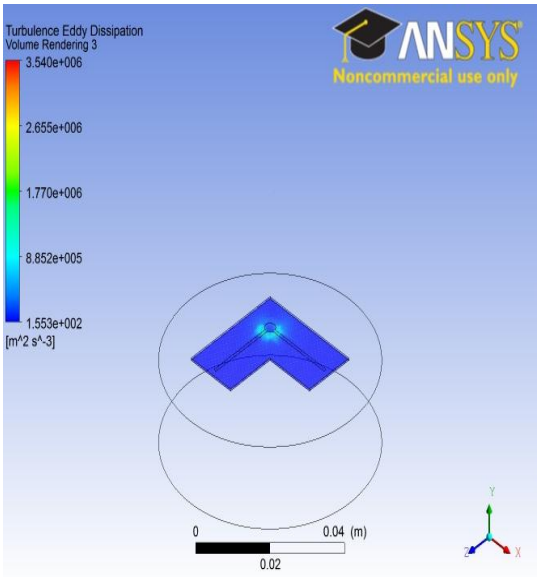

Fig. 4.23: Turbulence Eddy Dissipation of Model 4 with an inlet velocity 36m/s.

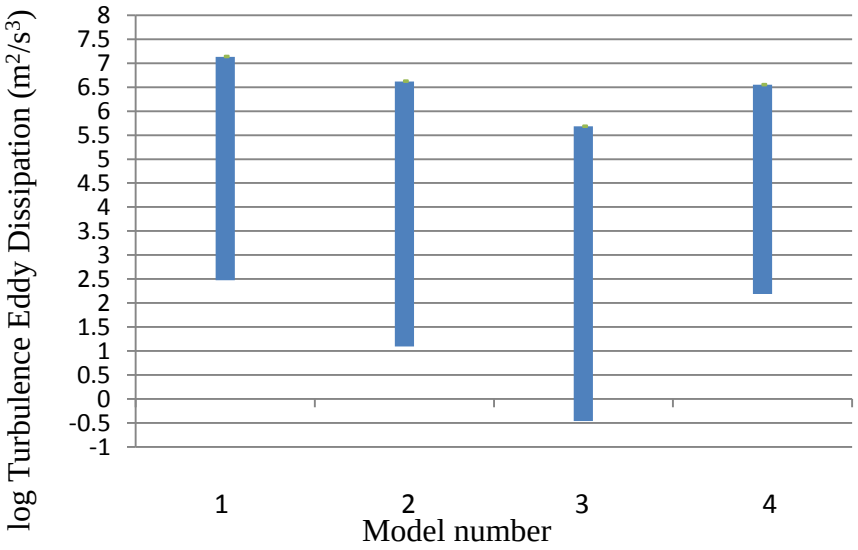

Fig. 4.24: Turbulence Eddy Dissipation variations of all the four Models with an inlet velocity 36 m/s

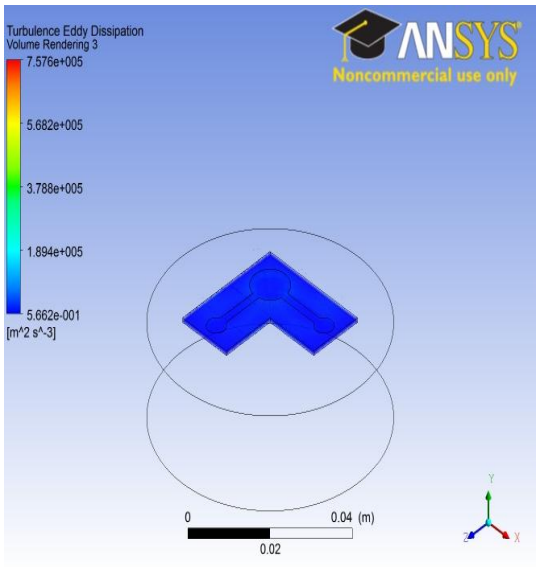

Fig. 4.25: Turbulence Eddy Dissipation of Model 3 with an inlet velocity 43m/s.

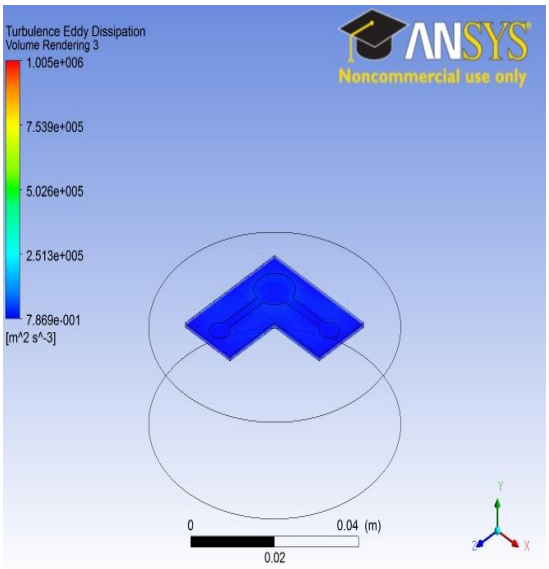

Fig. 4.26: Turbulence Eddy Dissipation of Model 3 with an inlet velocity 48m/s.

4.6. EFECT ON TEMPERATURE

Figs. 4.27, 4.28, 4.29 and 4.30 are the temperature distribution within the brine solution only in the IEG for Models 1, 2, 3 and 4 with an inlet velocity of 36 m/s respectively. All plots are plotted with a common scale of 298 to 400K. Since, the boiling point of brine solution is 373K, if temperature at any point goes beyond this limit, the electrolyte start to boil resulting in reduction in conductivity. This effect is more pronounce near the edges of the tool in the direction of the flow. In Model 1, the temperature throughout IEG is more than the boiling temperature. At the edge of the tool, the temperature is around 825K, where the electrolyte in that region starts to boil and the analysis is not valid.

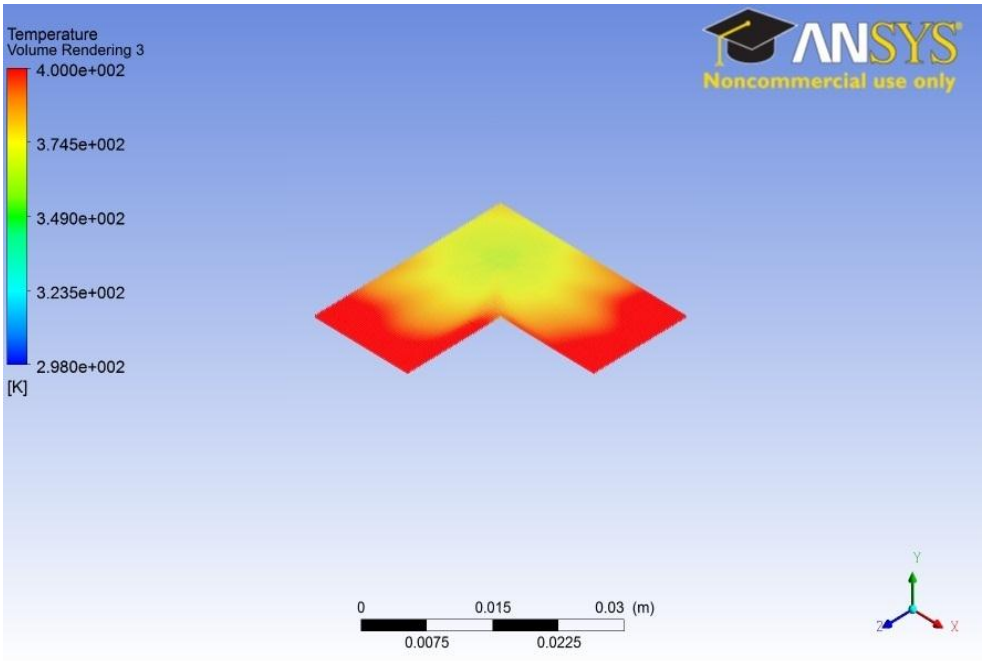

Fig. 4.27: Temperature distribution of Model 1 with an inlet velocity 36m/s

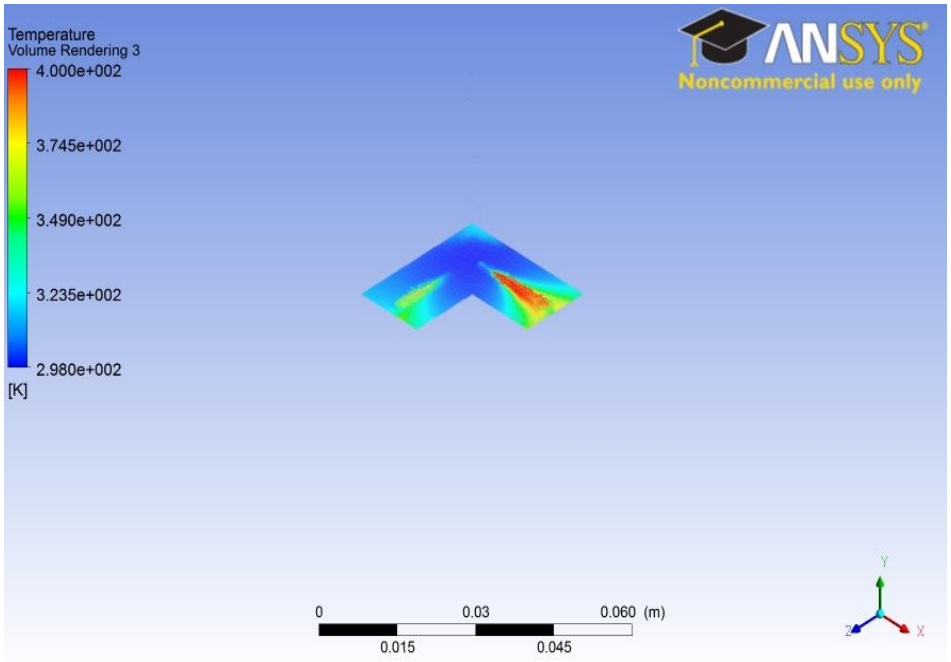

Fig. 4.28: Temperature distribution of Model 2 with an inlet velocity 36m/s

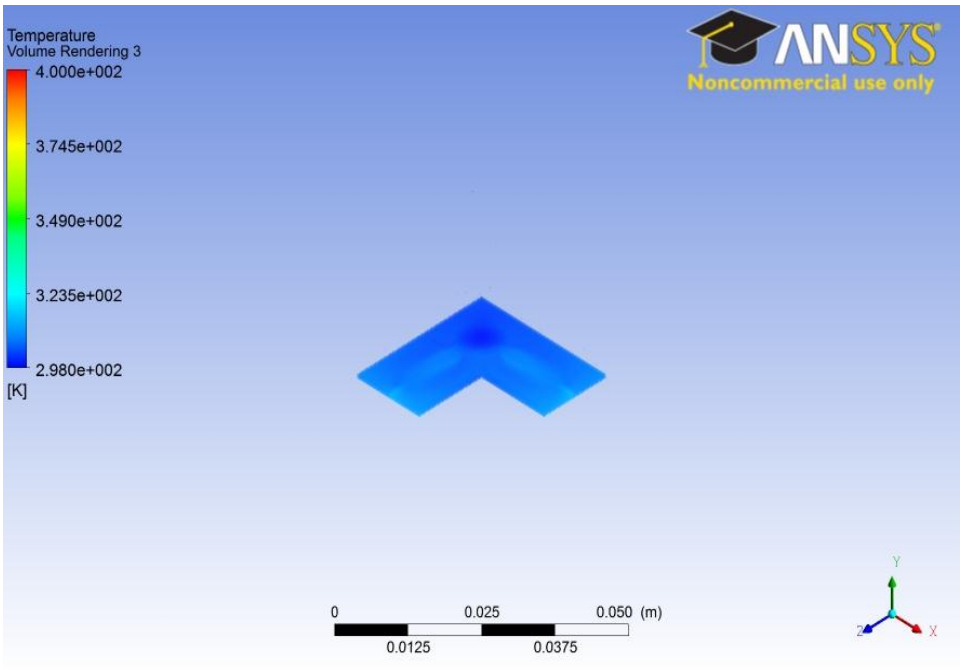

Fig. 4.29: Temperature distribution of Model 3 with an inlet velocity 36m/s

In case of Model 2, the temperature starts to rise in IEG after a small distance from the central hole within the slot. Maximum temperature obtained in this model is 420K. From the streamline plot (Fig. 4.8), it understood that at this region flow of electrolyte is not proper that is why it suddenly starts to increase. In Model 3, the temperature variation is very much less compared to other models. That is because of good flow pattern and uniform current density distribution. Maximum temperature obtained in this model is 315K. So here there is no chance of electrolyte boiling. In case of Model 4, the temperature distribution is not uniform and the maximum temperature is coming around 382K on the workpiece, which is not visible in 3D view. The electrolyte is IEG is showing evidence of boiling.

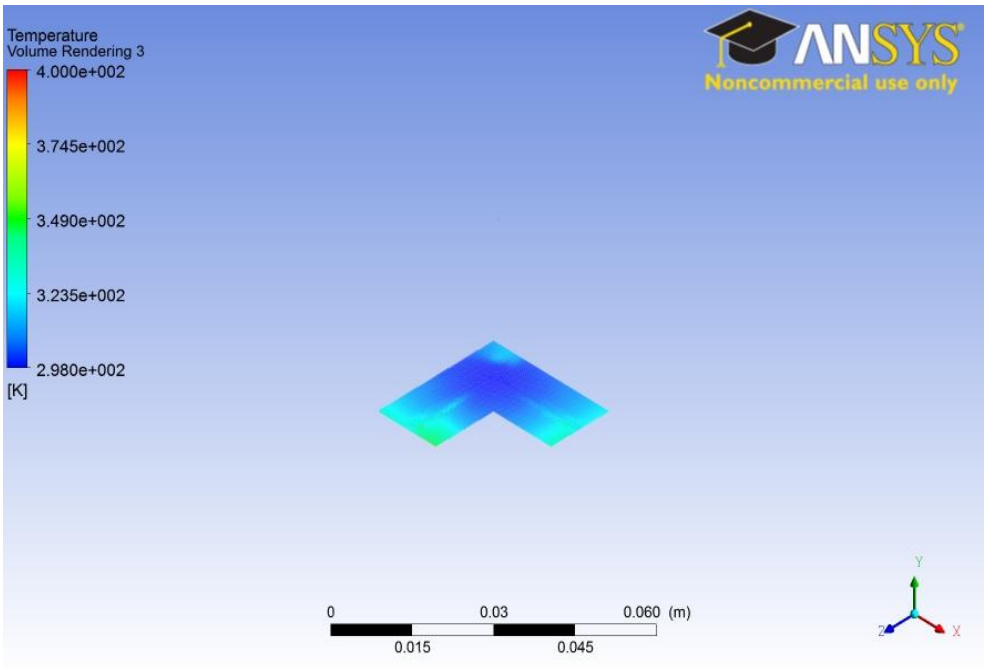

Fig. 4.30: Temperature distribution of Model 4 with an inlet velocity 36m/s

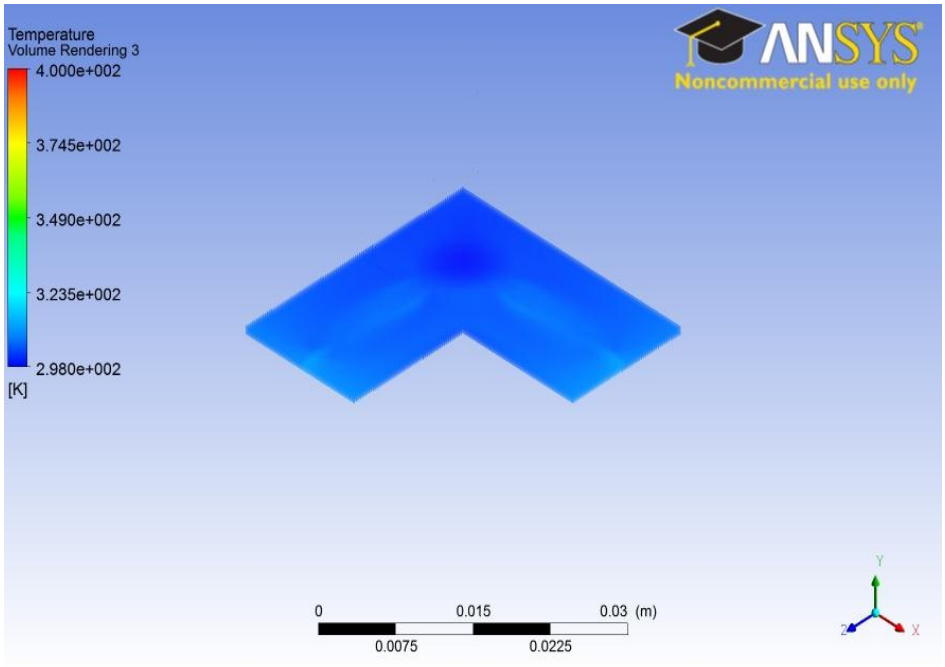

Fig. 4.31: Temperature distribution of Model 3 with an inlet velocity 43m/s

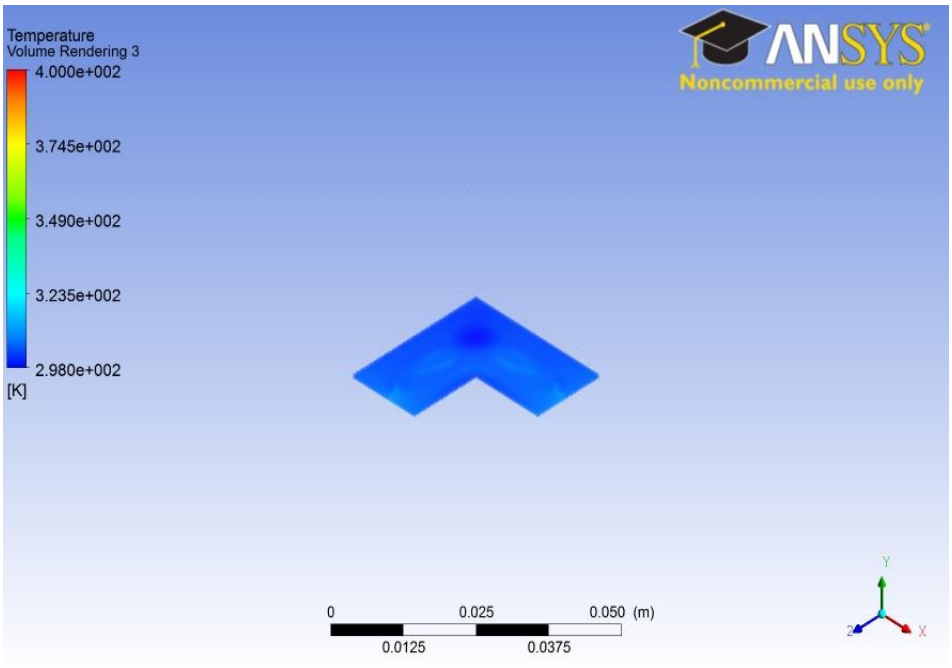

Fig. 4.32: Temperature distribution of Model 3 with an inlet velocity 48m/s

From the above discussion, it can be understand that Model 3 is the best, so we continue the simulation of Model 3 with increasing inlet velocities 43 m/s and 48 m/s. Distribution of temperature with 43 and 48 m/s velocities are shown in Fig. 4.31 and 4.32, respectively. The maximum temperatures for these analyses are 312K and 311K, respectively. From these results, it can be concluded that maximum temperature obtained in various models show decreasing trend with increasing inlet velocity.

4.6.1. INFLUENCE ON MAXIMUM TEMPERATURE WITH IN THE IEG

Fig. 4.33 is the graph plotted maximum temperature versus inlet velocity for various models. Maximum temperature for the inlet velocities 36, 43 and 48 m/s are plotted in this graph. In Model 1, the maximum temperature is drastically decreasing from 825K to 338 K that is because with lower flow rate of electrolyte, the heat dissipation is not adequate in IEG resulting in very

high temperatures. And the maximum temperature is in Model 1 is 333K with inlet velocity 48 m/s.

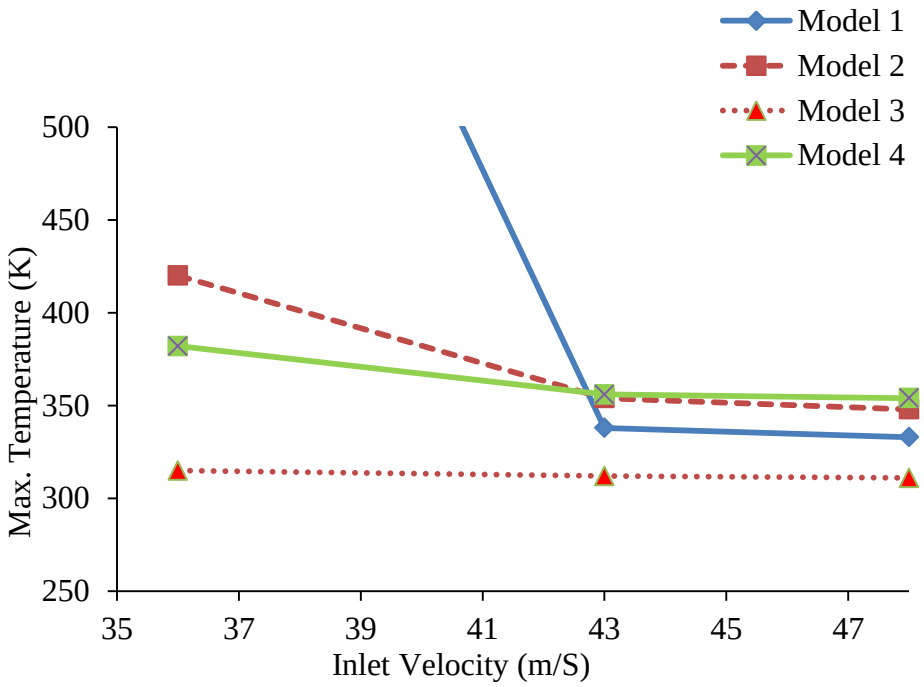

Fig. 4.33: Maximum Temperature versus inlet velocities graph

In the case of Model 2, the maximum temperature is decreasing form 420 to 354 K and from 354 to 348K when inlet velocity is increasing. The maximum temperature is smoothly decreasing first from 315 to 312K then to 311 for Model 3. Here, the flow is smooth and turbulence also less, hence the variations in the maximum temperature is less. In case of Model 4, it decreases first from 382 to 356 K then to 354K with increasing inlet velocity. The maximum temperature slopes of models are not similar in nature and the threshold inlet velocity required to prevent the electrolyte from boiling depends on the tool design. From Fig. 4.33, it can understand that maximum temperature in Model 3 is much less than other models and also less than the boiling

temperature, i. e., 373K. From these discussions, it understood that the models other than Model 3 are having electrolyte boiling tendency with inlet velocity lower than 43 m/s.

4.7. EFFECT ON CURRENT DENSITY

Figs. 4.34, 4.35, 4.36 and 4.37 are the current density distribution for Model 1, 2, 3 and 4, respectively, with an inlet velocity 36 m/s. In ECM process, the current density distribution is having immense importance because MRR is purely depended on the current density within the IEG. In Model 1, the current density is varying from 4.3436×10^{2} to 2.288×10^{5} A/m^2 and it is not uniform because of insufficient electrolyte flow. There is some current flowing beyond the tool's foot print in the workpiece which is because of stray current. The current density rapidly decreases to a minimum value that is evident from Fig. 4.34.

In case of Model 2, the current density is varying from 1.313×10^{2} to 1.879×10^{5} A/m^2. It is also having non-uniform current density distribution. But in Model 3, the current density distribution is more or less uniform throughout workpiece surface, that will result in higher MRR and good machined surface. Current density in the workpiece is various from 5.84×10^{3} to 1.356×10^{6} A/m^2. From the velocity profile, it can be understood that there is less passivated area in this model that is why a uniform current density variation is obtained. Model 4 also showing almost similar distribution pattern like Model 2. Current density within the workpiece is various from 5.572×10^{2} to 1.868×10^{5} A/m^2 for Model 4.

Fig. 4.38 is the chart plotted variation of current density in the tool foot print versus various models. It gave better idea about the variation of current density in each four models with an inlet velocity 36 m/s. the Current density value is more in case of Model 1 compared to other

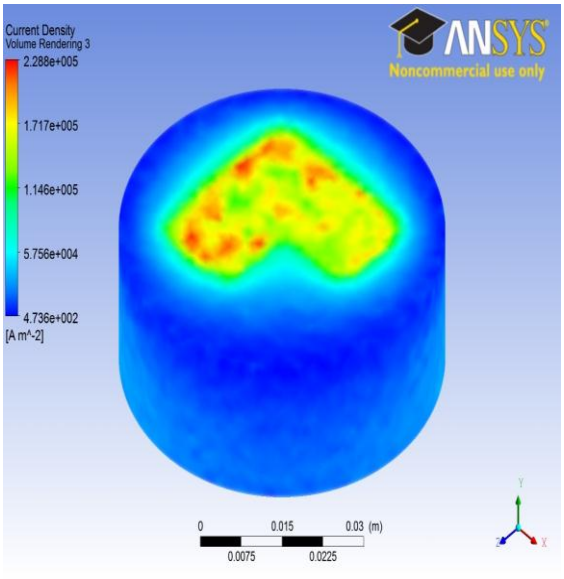

Fig. 4.34: Current density distribution of Model 1 with an inlet velocity 36m/s.

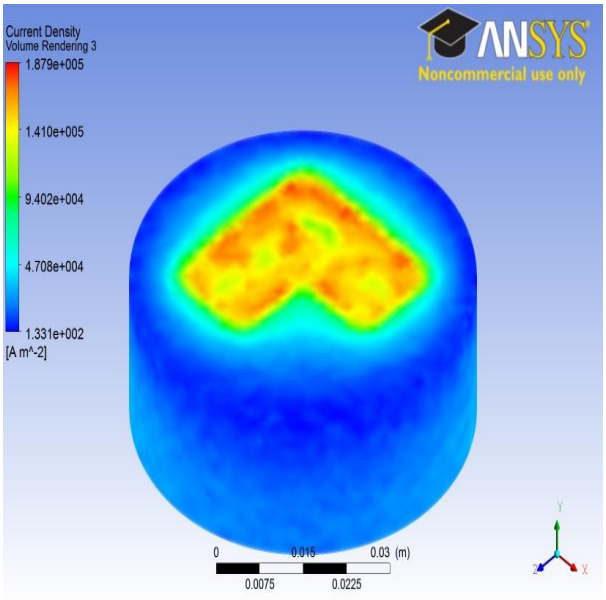

Fig. 4.35: Current density distribution of Model 2 with an inlet velocity 36m/s.

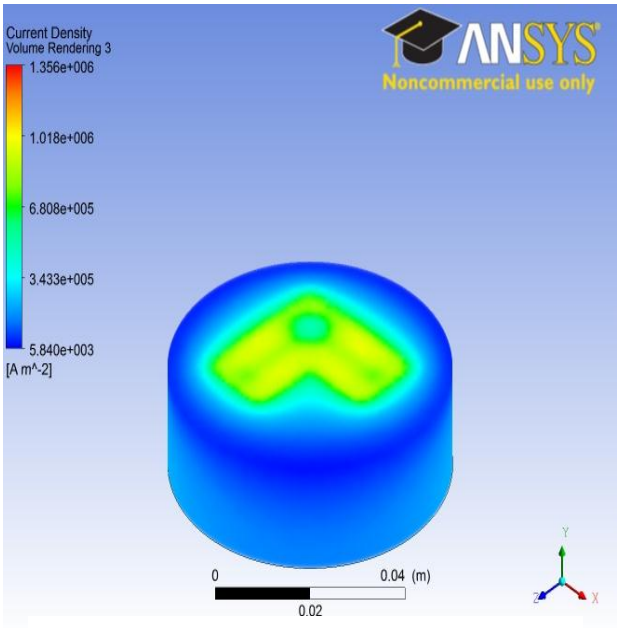

Fig. 4.36: Current density distribution of Model 3 with an inlet velocity 36m/s.

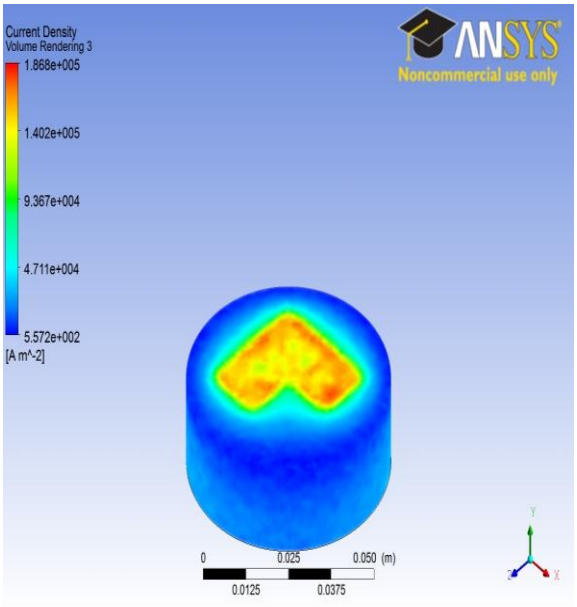

Fig. 4.37: Current density distribution of Model 4 with an inlet velocity 36m/s.

models and distribution of current density within the workpiece is uniform throughout the tool foot print area. There are not much variation in current densities for Model 1, 2 and 4.

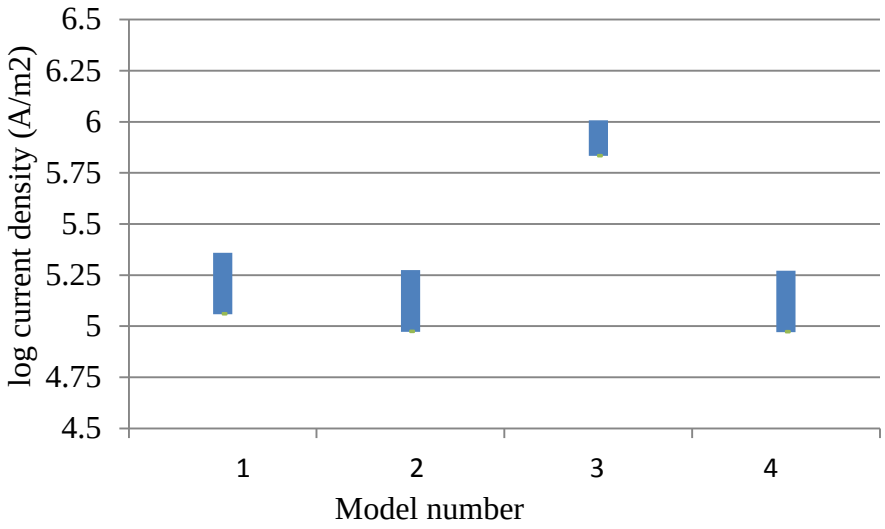

Fig. 4.38: Current density variations of all the four Models with an inlet velocity 36 m/s.

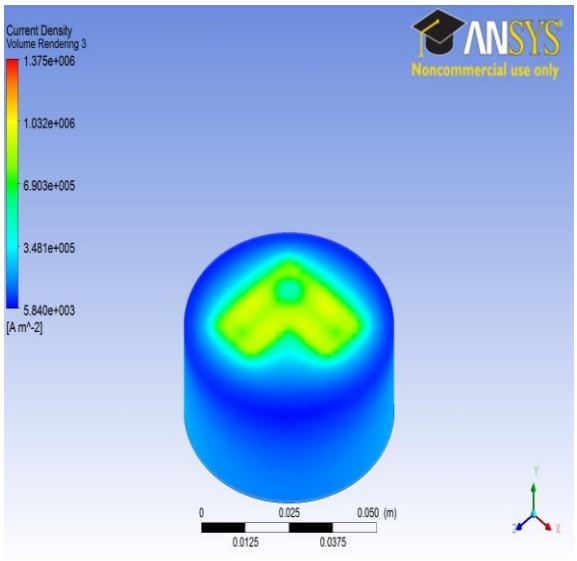

Fig. 4.39: Current density distribution of Model 3 with an inlet velocity 43m/s.

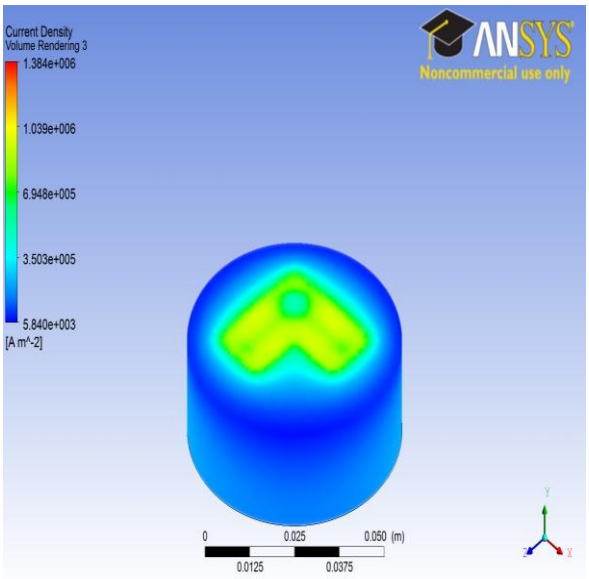

Fig. 4.40: Current density distribution of Model 3 with an inlet velocity 48m/s.

The temperature rise in Model 3 is less compared to other models and the velocity profile is also showing no passivation. There is no eddy formation and turbulence is much less for the design of Model 3. Hence, it can be concluded that Model 3 is the best among all four tool designs. So we continue the simulation of Model 3 with increasing inlet velocities 43 m/s and 48 m/s. Distribution of current density with 43 and 48 m/s velocities are shown in Figures 4.39 and 4.40, respectively. These plots are also distributing current density more or less uniformly throughout the area. In Figure 4.39 current density is varying from 5.84×10^{3} to 1.375×10^{6} A/m^2 and in Figure 4.40, it varies from 5.84×10^{3} to 1.384×10^{6} A/m^2. Hence, better current density distribution is observed for Model 3 than other models with increasing inlet velocity.

4.7.1. INFLUENCE ON AVERAGE CURRENT DENSITY

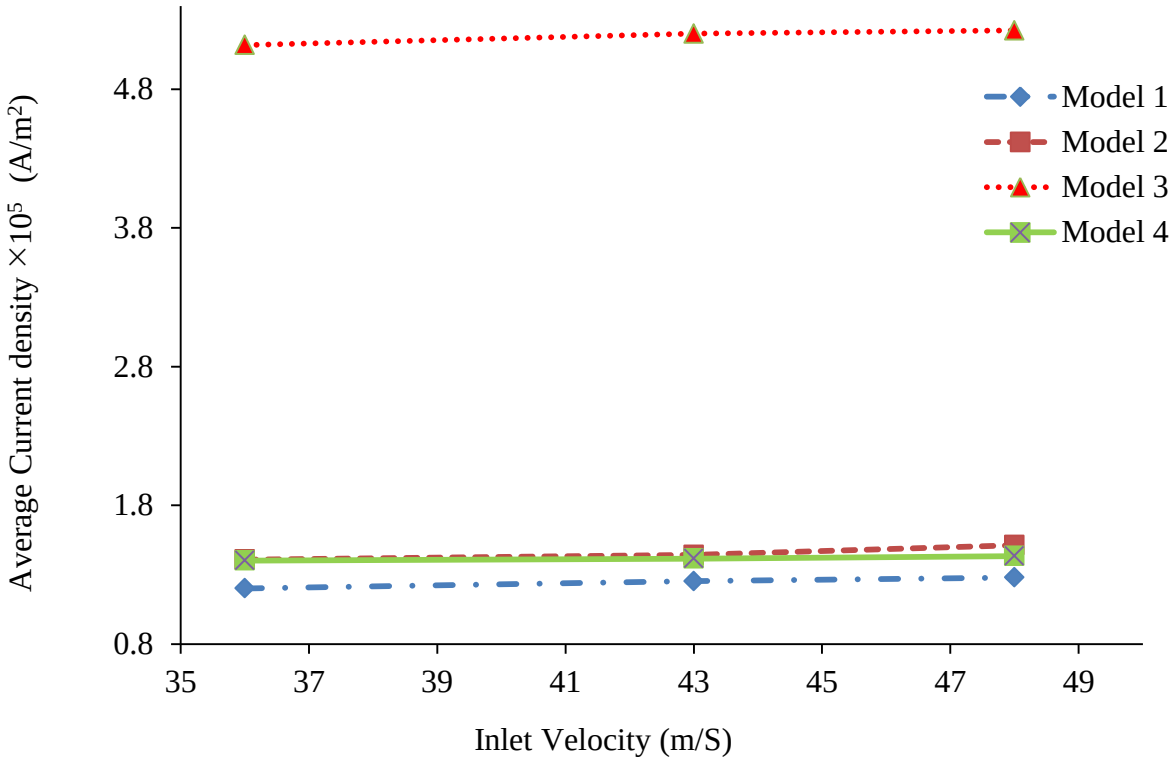

Fig. 4.41: Average current density vrs inlet velocity graph.

Fig. 4.41 is the graph plotted for the average current density versus inlet velocity for the four models. For Model 1, the slope of the average current density is 0.0075 A in the range of inlet velocity 36 to 43 m/s and the same for 43 to 48 m/s is 0.0052 A. In Model 2 and Model 4, the change in average current density is comparable with that of Model 1. In the case of Model 3, the slope is 0.01154 A and 0.00484 A for the range of inlet velocity 36 to 43 m/s and 43 to 48 m/s, respectively. Here the flow is smooth and turbulence also less, so due to these all reasons variations in average current density doesn't have much variation. Fig. 4.41, it can be understood that the average current density for Model 3 is more than other models.

4.8. INFLUENCE ON FINAL SHAPE

The final shape of the workpiece after 30s of machining with an inlet velocity 36 m/s for Models 1 is shown in Fig. 4.42. The cavity has flat irregular surface with a single boss that is because of stagnation phenomenon near the central hole. The effect of stray machining is also visible in this figure that is shown as the curved edges of L-shaped tool. In Fig. 4.43, for Model 2, the surface is irregular in nature due to wrong groove design and material removal is also less in this. In Model 3, the cavity is more and irregularities due to boss formation are present (Fig. 4.44). In case of Model 4, it's clear from Fig. 4.45 that the surface irregularities are more. Material removal is the highest in case of Model 3. Simulation process was continued for Model 3 with various inlet velocities 43 and 48 m/s and is presented in Figs. 4.46 and 4.47, where the cavity impression is increasing.

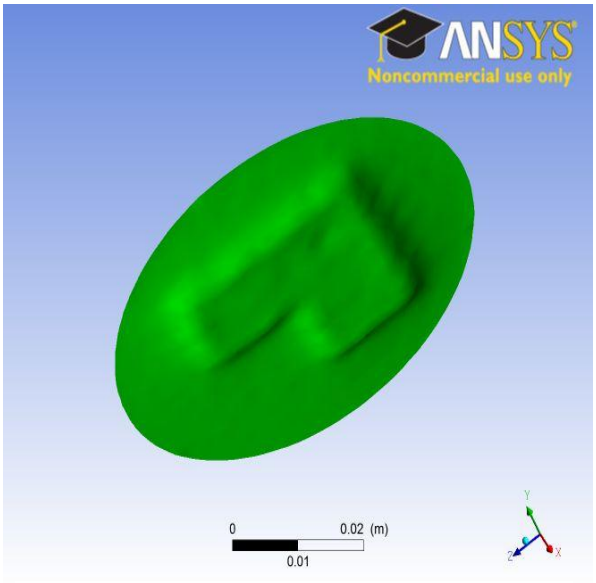

Fig. 4.42: Workpiece top surface after 30 s machining of Model 1 with an inlet velocity 36m/s.

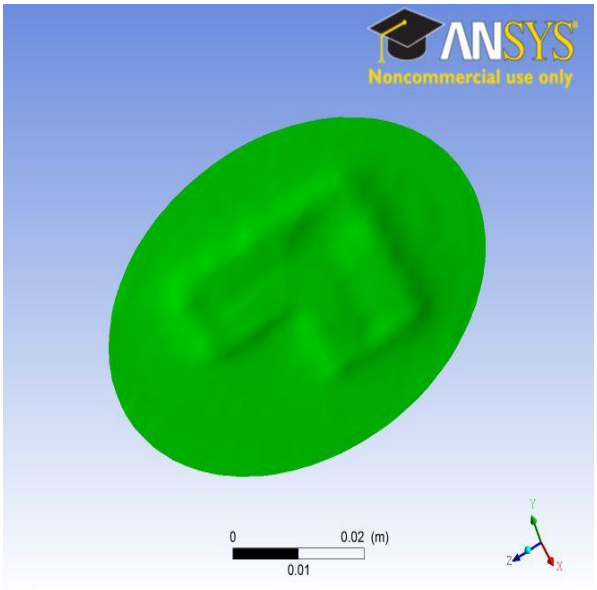

Fig. 4.43: Workpiece top surface after 30 s machining of Model 2 with an inlet velocity 36m/s.

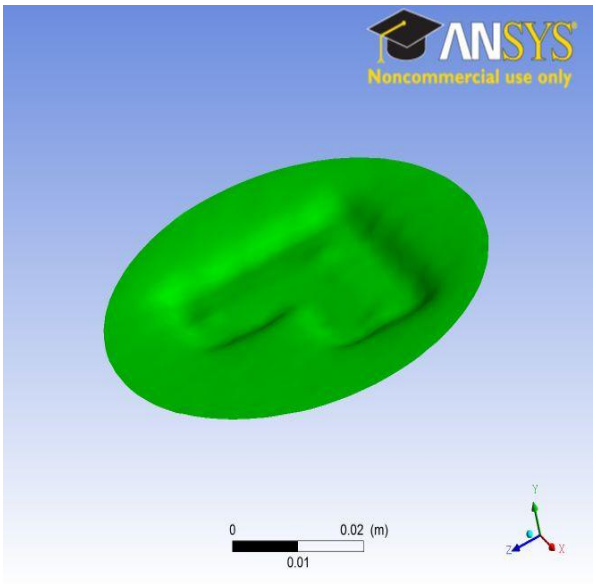

Fig. 4.44: Workpiece top surface after 30 s machining of Model 3 with an inlet velocity 36m/s.

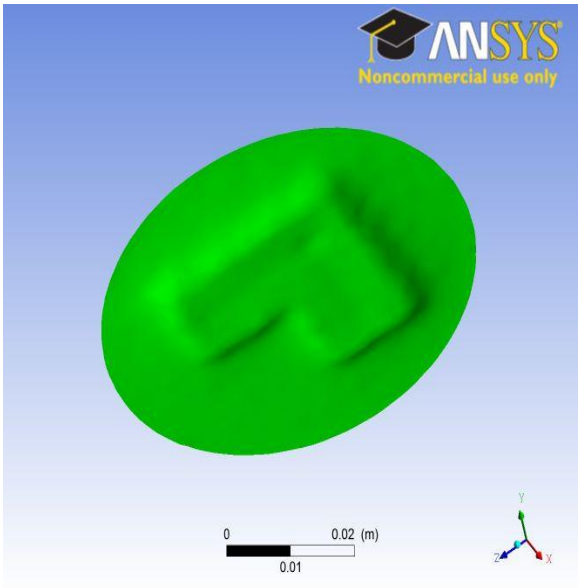

Fig. 4.45: Workpiece top surface after 30 s machining of Model 4 with an inlet velocity 36m/s.

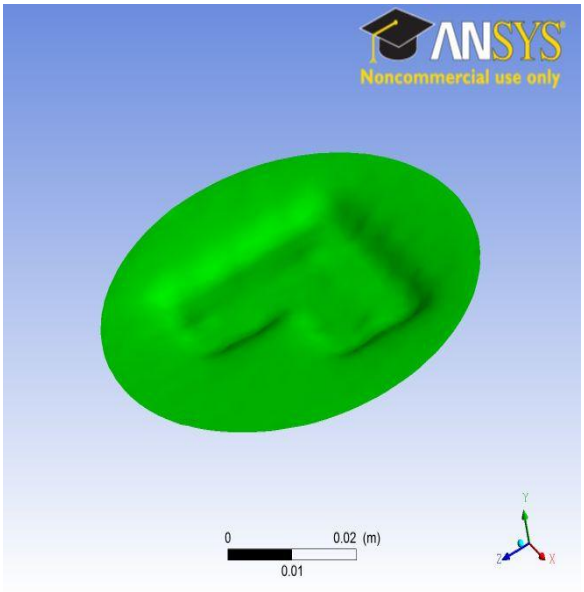

Fig. 4.46: Workpiece top surface after 30 s machining of Model 3 with an inlet velocity 43 m/s.

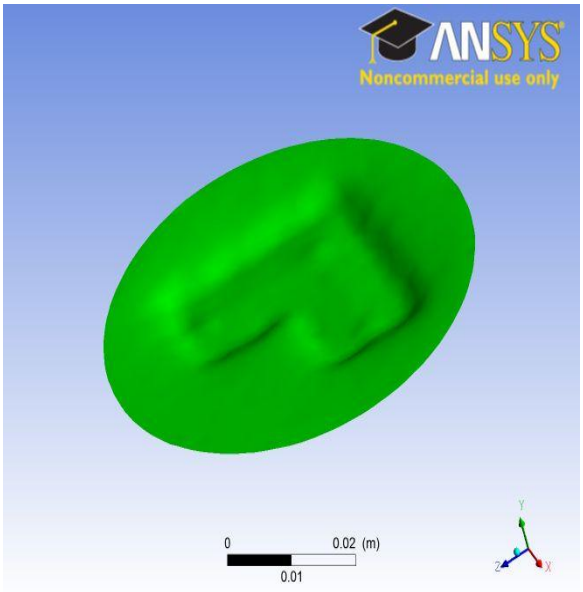

Fig. 47: Workpiece top surface after 30 s machining of Model 3 with an inlet velocity 48 m/s.

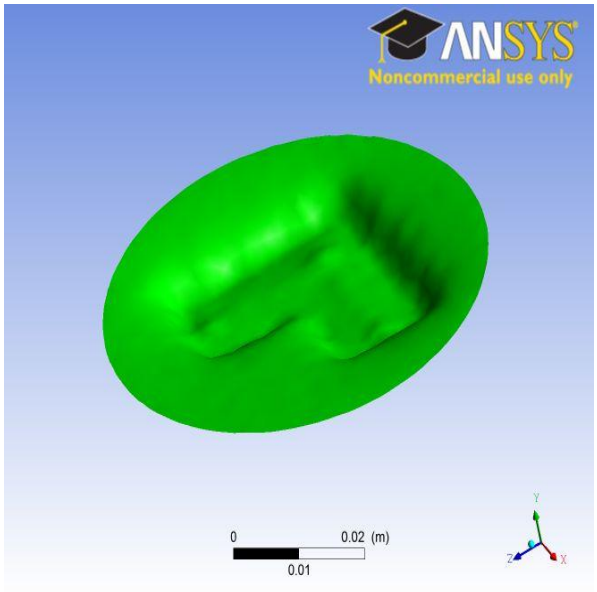

Fig. 4.48: Workpiece top surface after 60 s machining of Model 3 with an inlet velocity 36 m/s.

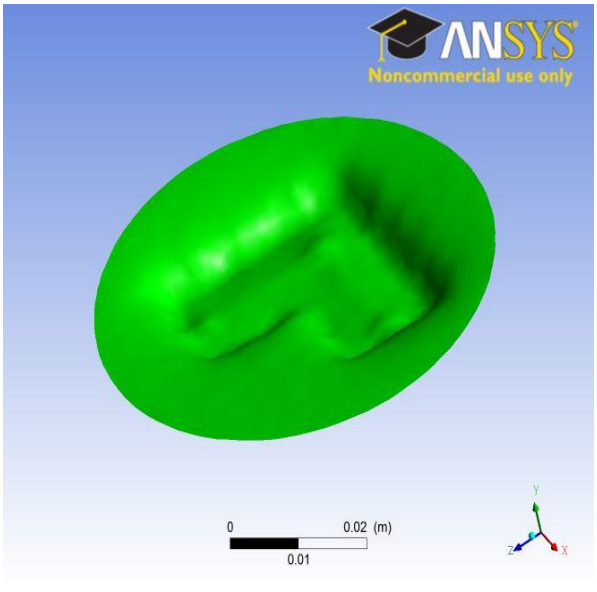

Fig. 4.49: Workpiece top surface after 60 s machining of Model 3 with an inlet velocity 43 m/s.

Fig. 4.48, 4.49 and 4.50 are final shapes of workpiece after 60 s machining with an inlet velocity 36, 43 and 48 m/s, respectively, for Model 3. These are also showing that MRR is increasing a bit with increasing inlet velocities.

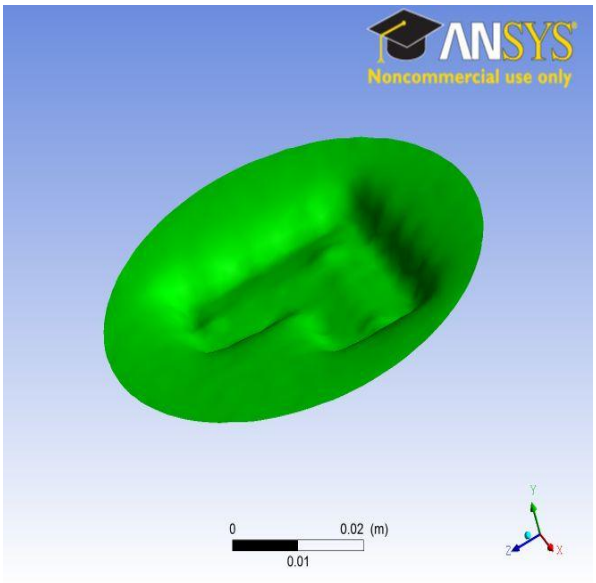

Fig. 4.50: Workpiece top surface after 60 s machining of Model 3 with an inlet velocity 48 m/s.

4.9. INFLUENCE ON MATERIAL REMOVAL RATE

Fig. 4.51 is the graph plotted MRR against inlet velocity for various models. For Model 1, the MRR is much less than that of other models for all velocities. This can be attributed to passivation effect when material removal from these areas is less. MRR is increasing from 0.029×10^{-6} m^3/s to 0.0301×10^{-6} m^3/s and to 0.0305×10^{-6} m^3/s. In Model 4, the MRR is more than Model 1 and it increases first from 0.029×10^{-6} m^3/s to 0.031×10^{-6} m^3/s and to 0.0315×10^{-6} m^3/s. In Model 2, MRR is more than Model 4 that increases from 0.0291×10^{-6} m^3/s to 0.0318×10^{-6} m^3/s and to 0.0322×10^{-6} m^3/s. Both Models having grooves but Model 2 don't have any sharp

ends. That is the reason for increasing MRR. From the graph it is understood that Model 3 has more MRR. Reason for that are uniformity in current density distribution and less passivation. MRR is increase from 0.0319×10^{-6} m^3/s to 0.0327×10^{-6} m^3/s and finally to 0.0333×10^{-6} m^3/s.

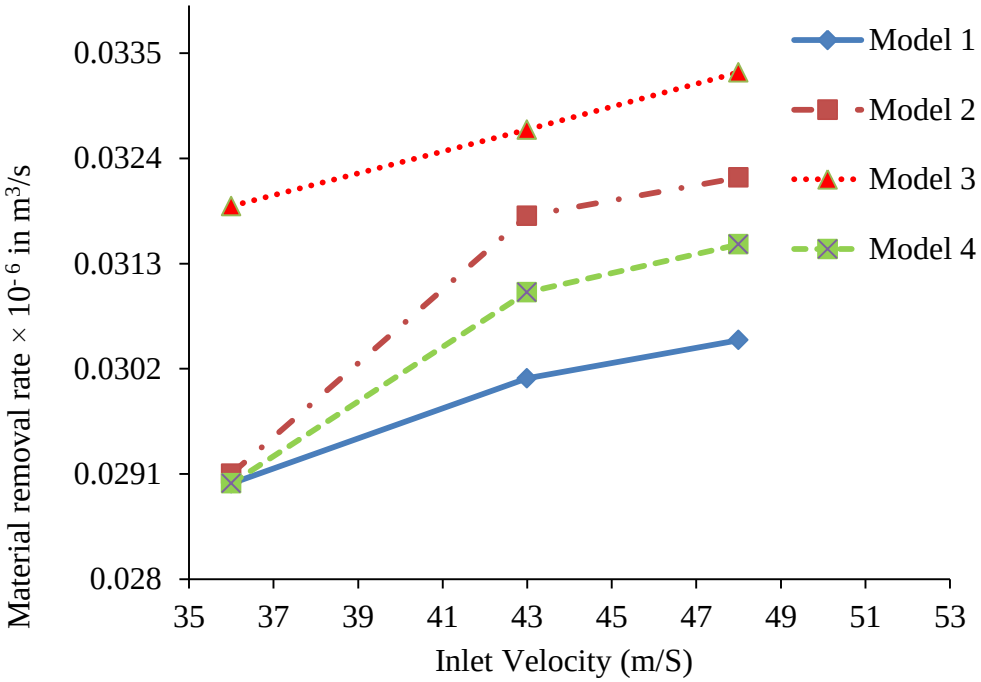

Fig. 4.51: Material removal rate versus Inlet velocities

4.10. CONCLUSIONS

The study of velocity profile within the IEG, current density in the workpiece, temperature variation in the inter electrode gap, streamline flow, turbulence, final shape change of work piece surface and material removal like parameters explained that Model 3 is best among the consideration. The velocity profile of all models explains that Model 3 has less passivation compared to other models. The streamlines only for Model 3 are properly distributed in the IEG

resulting in less passivation. Turbulence in Model 3 is less it is explained by turbulent kinetic energy and turbulent eddy dissipation. The maximum temperature for Model 3 is much less than other models, where as the other models requires minimum 43 m/s inlet velocity to avoid boiling of electrolyte. The above mentioned parameters are affecting the current density distribution in the models, results shows that Model 3 has higher current density. Therefore Model 3 has higher MRR that results larger cavity in the workpiece.

CHAPTER 5

CONCLUSIONS

Flow pattern analysis of electrochemical machining with L-shaped tool is giving better idea of velocity distribution, temperature profile, turbulence etc. in the inter electrode gap. In this analysis, a cylindrical Iron workpiece, Copper tool and 20% brine solution as electrolyte was considered. Four tools with different slot design were modeled using Design Modeler in ANSYS 13.0 and analyzed. All models are meshed using mesh module with an orthogonal quality of more than 0.9 which ensure these models will give good results. All models are analyzed with inlet velocities 36, 43 and 48 m/s and RMS value is 1×10^{5} is used as convergence criteria.

6.1.1 MAJOR CONCLUSIONS

i. The maximum temperature in IEG for all models has a decreasing tendency with respect to the increase in inlet velocities.

ii. The maximum current density has increasing tendency with respect to increase in inlet velocities.

iii. MRR and turbulence also increase in inlet velocities.

iv. Tendency of passivation is decreasing in case of all models with increasing velocity.

v. Model 3 is the best tool design from among the four models evaluated.

6.1.2 SCOPE FOR FUTURE WORK

i. This work done in steady state mode, transient mode simulations are also possible with these models.

ii. Experimental validation of this work can do with the optimum model got from this analysis.

iii. Instead of mass pure material alloy material can use as electrodes.

iv. Solid fluid interaction with reactions can include in this model.

v. Final shape of these simulations can call back as an input of the next simulation.

ANNEXURE A

A.1. SPECIFICATION OF ECM MCHINE

The specifications for some of the parameters involved in the ECM are explained in the Table A1. Boundary conditions are fixed according to this specification.

Table A.1: Specification of Electrochemical Machining

Sl. No	**Parameters**	**Specifications**
1	Working gap	0.05-0.8 mm
2	Current density	5-100 A/cm^2
3	Voltage	5-30 V
4	Current	50-40,000 amp
5	Temperature	30-80 ^0C
6	Velocity	5-50 m/s
7	Maximum material removal rate	15×10^3 mm^3/min
8	Inlet Pressure	0.15-3MPa
9	Outlet Pressure	0.1-0.3MPa
10	Feed Rate	0.1-20mm/min
11	Electrolyte Used	Brine solution, Sodium nitrate
12	Specific power consumption	$7w/mm^3/min$
13	Accuracy and surface finish	0.02 mm, 0.4μm

14	Critical parameters	Voltage, current, feed rate, electrolyte, and electrolyte conductivity.
15	Application	Machining hard material, machining complex shaped parts like blind complex cavities, curved surface through cutting etc.
16	Limitation	High specific energy consumption, not applicable with electrically non-conducting materials and for job with small dimensions.
17	Mechanical properties	Stress free machining, reduce tool wear
18	Surface properties	No thermal damage

ANNEXURE B

THEORIES IN CFX

ANSYS software is constructed based on some principles and theories. Some theories related to this work are discussed in the following sections.

B.1. ELECTRO HYDRODYNAMIC THEORY

The interaction between CFD and Computational Electro-Magnetics (CEM) through the body forces that result due to the interaction between electromagnetic field and fluid motion. Electro Hydrodynamics is the study of interaction between magnetic fields and electrically charged fluids. Computational Electro-Magnetics (CEM) based on:

i. Maxwell's equation and further relations.

ii. Material relations for permittivity, conductivity and permeability.

The Coulomb force acting on the fluid along the applied electric field is given by the Equation 3.15.

$$F_{E\,Mag} = qE \qquad (B.1)$$

In quasi static magnetic hydrodynamics (MHD) and EHD models the electric field can be either solved by using electric potential equation or user specified manner. Momentum and energy sources equations are solved through Lorentz fore and Joule heating.

B.2. GRID GRAPHIC INTERFACE (GGI)

This is a method used for connecting meshes in the interface zone. Control surface approach is used to connect the interaction in GGI method. Physically based interface algorithm is used in this method. This will help to change the grid topology and physical distribution across the interface. This method is also providing surface trimming option. Treatment in the interface are fully implicit and fully conservative in mass, momentum and energy. Multi grid solver can also apply directly to the problem having GGI connection. GGI interface having the following attributes,

i. Strict conservation for all fluxes is maintained across the interface.
ii. Interface treatment is fully implicit.
iii. It is applicable for all type of flows.
iv. Any number of GGI connections is possible in the domain.

B.3. PARALLEL SOLVER METHOD

Parallel solver implementation is based on SPMD model. This process is divided into steps,

i. Partitioning step: mesh is divided into segments. Partitions are generally element based or node based.

ii. Running step: mesh partitions are solved by using different processors.

In this simulation ‘Metis’ type algorithm is used. It is a most advanced mesh partition algorithm. Basic idea behind this algorithm is a graph built containing the topology information of the mesh to be partitioned. This graph is first coarsened down to a few hundred vertices. Bisection of the resulting much coarser graph is calculated then the resulting partitions are projected back onto the original graph, by consecutively refining the graph. With this algorithm we can partition the domain separately or combined manner.

B.4. WAY TO INPUT k-Ɛ MODELS

For enabling this model we must give reasonable value for either the turbulent intensity or k and ε at the inlet. If you have no idea about the turbulence level in your simulation then should use well-chosen values for turbulent intensities and length scale. Nominal turbulence intensities are ranges from 1 to 5%. If we know the approximate value for incoming intensity then we can specify this with appropriate length scale. In case of internal flow a fraction of inlet diameter is a good approximation for length scale. If you want to give the approximate values for k and ε we can use the relations shown in Equations 3.16 and 3.17.

$$k = \frac{3}{2} i^2 U^2 \qquad (B.2)$$

$$\varepsilon = \frac{k^{3/2}}{0.3 D_h} \qquad (B.3)$$

D_h is the hydraulic diameter in the inlet. These relations are applicable only for small inlet diameter. In turbulent simulation, the nature of flow in the upstream region of IEG would be of interest which may affect the turbulence intensity.

Options available in the inlet region are,

i. Default intensity and auto compute length.

   It is taking the default value 3% for turbulent intensity with a compute length scale to approximate inlet values of k and ε. Auto computation length is not suitable for external flow.

ii. Intensity and auto compute length scale.

   This is allowed to specify the intensity value but length scale calculated automatically. The allowable value for turbulent intensity is restricted from 1 to 10%. Here also auto computation length is not suitable for external flow.

iii. Intensity and length scale.

In this we can specify the value of intensity and length scale from which values of k and ε are calculated.

iv. Low (Intensity = 1%)

This defines a 1% intensity and viscosity ratio (μ_t/μ) = 1.

v. Medium (Intensity = 5%)

This defines a 5% intensity and viscosity ratio (μ_t/μ) = 10.

vi. High (Intensity = 10%)

This defines a 10% intensity and viscosity ratio (μ_t/μ) = 100.

vii. Specified intensity and eddy viscosity ratio.

Here we can specify the values for intensity and eddy viscosity ratio directly.

viii. K and ε

Here we can specify the values for K and ε directly.

ix. Zero gradient

Use this setting for fully developed turbulence condition.

REFERENCES

1. **Purcar, M., Bortels, L., Bossche and B.V.D. Deconinck, J.,** (2004). 3D electrochemical machining computer simulations, *Journal of Materials Processing Technology*, 149, 472–478.

2. **Krimmelbein, N. and Radespiel, R.,** (2009). Transition prediction for three-dimensional flows using parallel computation, *Journal of Computers & Fluids*, 38, 121–136.

3. **Labib, A.W., Keasberry, V.J., Atkinson, J. and Frost H.W.,** (2011). Towards next generation electrochemical machining controllers, A fuzzy logic control approach to ECM. *Journal of Expert Systems with Applications*, 38, 7486–7493.

4. **Guermond, J.L. and Minev, P.D.,** (2011). A new class of massively parallel direction splitting for the incompressible Navier–Stokes equations. *Computer. Methods Application in Mechanical Engineering*, 200, 2083–2093.

5. **Kozak, J.,** (1998). Mathematical model for computer simulation of electrochemical machining processes, *Journal of Material Processing Technology*, 76, 170-175.

6. **Mount, A.R., Clifton, D., Howarth, P. and Sherlock, A.,** (2003). An integrated strategy for materials characterization and process simulation in electrochemical machining, *Journal of Materials Processing Technology*, 138, 449–454.

7. **Gambaryan, T., Roisman, and Stephan, P.,** (2006). A numerical model for the thermocapillary flow and heat transfer in a thin liquid film on a micro structured wall, *International Journal of Numerical Methods for Heat & Fluid Flow*, 17,247-262.

8. **Kozak, J., Chuchro, M., Rusza, A. and Karbowsk, K.,** (2000). The computer aided simulation of electrochemical process with universal spherical electrodes when machining sculptured surface, *Journal of Materials Processing Technology, 107, 283-287.*

9. **Bortels, L., Purcar, M., Bossche, B.V.D. And Deconinck, J.,** (2004). A user-friendly simulation software tool for 3D ECM. *Journal of Materials Processing Technology*, 149, 486–492.

10. **Pattavanitch, J., Hinduja, J. and Atkinson, J.,** (2010). Modelling of the electrochemical machining process by the boundary element method. *CIRP Annals - Manufacturing Technology*, 59, 243–246.

11. **Pons, M., and Que´re, P. L.,** (2006). Modeling natural convection with the work of pressure-forces: a thermodynamic necessity. *International Journal of Numerical Methods for Heat & Fluid Flow*, 17, 322-332.

12. **Dabrowski, L., and Paczkowski, T.,** (2011). Computer simulation of Two-dimensional Electrolyte flow in Electrochemical Machining. *Russian journal of electrochemistry*, 41,102–110.

13. **Wang, G., Yang, Y., Zhang, H and Xia W.,** (2007). 3-D model of thermo-fluid and electrochemical for planar SOFC, *Journal of Power Sources*, 167, 398–405.

14. **Ratkovich, N., Chanb, C.C.V., Berubeb, P.R. and Nopensa. I.,** (2009). Experimental study and CFD modelling of a two-phase slug flow for an airlift tubular membrane, *Journal of Chemical Engineering Science*, 64, 3576 – 3584.

15. **Dixona, A.G., Taskina, M.E., Nijemeislandb, M. and Stitt, E.H.,** (2011). Systematic mesh development for 3D CFD simulation of fixed beds:Single sphere study, *Journal of Computers and Chemical Engineering*, 35, 1171–1185.

16. **Kanarska, Y., Lomov, I. and Antoun, T.,** (2011). Mesoscale simulations of particulate flows with parallel distributed Lagrange multiplier technique. *Journal of Computers and Fluids*, 48, 16–29.

17. **Mcclesky, R.B.,** (2011). Electrical Conductivity of Electrolytes Found In Natural Waters from (5 to 90) °C. *Journal of Chemical and Engineering data*, 56, 317-327.

18. **Sian, S.,** (2011). CFD analysis of flow pattern in electrochemical machining, B.Tech. Project Report, *National Institute of Technology Rourkela*, Odhisa, India.

19. **Tu, J., Yeoh, G.H. and Liu, C.,** (2008). Computational Fluid Dynamics a practical approach, *Butterworth-Heinemann, Jordan Hill,* Oxford, UK.

20. **Ghosh, A. and Mallik, A.K.,** (2010). Manufacturing Science Second Edition, *East-West Press Private Limited,* New Delhi, India.

21. **Mishra, P.K.,** (2006). Nonconventional Machining, *Narosa Publications*, New Delhi, India.

22. **Jain, R.K.,** (2001). Production technology, *Khanna Publishers*, New Delhi, India.

23. ansys.com

24. wiki.answers.com

25. en.wikipedia.org

26. scribd.com

27. cfd-online.com

28. www.mece.ualberta.ca/tutorials/ansys